Geophys. J. Int. (2004) **159,** 842–862 doi: 10.1111/j.1365-246X.2004.02454.x

BARGEN continuous GPS data across the eastern Basin and Range province, and implications for fault system dynamics

Nathan A. Niemi,[1] Brian P. Wernicke,[1] Anke M. Friedrich,[1,*] Mark Simons,[1] Richard A. Bennett[2] and James L. Davis[3]

[1] *Division of Geological and Planetary Sciences, California Institute of Technology, Pasadena, CA* 91125, *USA. E-mail: niemi@gps.caltech.edu*
[2] *Department of Geosciences, University of Arizona, Tucson, AZ 85721, USA*
[3] *Harvard–Smithsonian Center for Astrophysics, Cambridge, MA* 02138, *USA*

Accepted 2004 July 26. Received 2003 March 25; in original form 2001 February 23

SUMMARY

We collected data from a transect of continuous Global Positioning System (GPS) sites across the eastern Basin and Range province at latitude 39°N from 1997–2000. Intersite velocities define a region ∼350 km wide of broadly distributed strain accumulation at ∼10 nstr yr^{-1}. On the western margin of the region, site EGAN, ∼10 km north of Ely, Nevada, moved at a rate of 3.9 ± 0.2 mm yr^{-1} to the west relative to site CAST, which is on the Colorado Plateau. Velocities of most sites to the west of Ely moved at an average rate of ∼3 mm yr^{-1} relative to CAST, defining an area across central Nevada that does not appear to be extending significantly. The late Quaternary geological velocity field, derived using seismic reflection and neotectonic data, indicates a maximum velocity of EGAN with respect to the Colorado Plateau of ∼4 mm yr^{-1}, also distributed relatively evenly across the region. The geodetic and late Quaternary geological velocity fields, therefore, are consistent, but strain release on the Sevier Desert detachment and the Wasatch fault appears to have been anomalously high in the Holocene. Previous models suggesting horizontal displacement rates in the eastern Basin and Range near 3 mm yr^{-1}, which focused mainly along the Wasatch zone and Intermountain seismic belt, may overestimate the Holocene Wasatch rate by at least 50 per cent and the Quaternary rate by nearly an order of magnitude, while ignoring potentially major seismogenic faults further to the west.

Key words: continental deformation, fault slip, normal faulting, Quaternary, satellite geodesy, stress distribution.

1 INTRODUCTION

Relative plate motion tends to be focused on discrete, rapidly moving faults, but, where one or both plates are continental, a significant fraction is also accommodated on complex, diffuse fault systems hundreds to thousands of kilometres wide. For example, of the 48–51 mm yr^{-1} of relative motion between the Pacific and North American plates in the southwestern USA, 35 mm yr^{-1} is accommodated in a zone <100 km wide along the San Andreas fault (Fig. 1). The remaining 13–16 mm yr^{-1}, or ∼25–30 per cent of the total, is distributed across a complex system of faults more than 1000 km wide, which includes the Basin and Range province (Fig. 2; e.g. Bennett *et al.* 1999).

Within the Basin and Range, faults with Quaternary (<1.6 Ma) slip rates of order 0.1–1.0 mm yr^{-1} are developed over a broad region, but historical seismicity is clustered on only a few of them. For example, the northern Basin and Range region contains several hundred fault segments with significant late Quaternary (<130 ka) slip, yet contemporary seismicity and large ($M \geq 6.5$) historical earthquakes are concentrated in two north-trending belts along or near the margins of the province, including the Eastern California seismic belt and Central Nevada seismic belt on the west, and the Intermountain seismic belt on the east (Fig. 2; Wallace 1984; Smith & Sbar 1974). The pattern of seismicity must be much more diffuse at longer timescales, because nearly every range-bounding fault has substantial Quaternary offset (Wallace 1987).

These observations pose the question: is contemporary strain accumulation focused in the seismically active belts, or is a significant fraction of it distributed across areas that are now relatively aseismic? At one extreme, seismicity and strain accumulation migrate together, such that at any given time the crust is deforming as a system of large, discrete subplates or microplates defined by seismicity, whose configuration changes with time to produce the appearance of continuous strain. At another, seismicity migrates across a region of spatially and temporally continuous strain accumulation, such that

*Now at: Institut für Geowissenschaften, Universität Potsdam, Potsdam 14469, Germany.

 © 2004 RAS

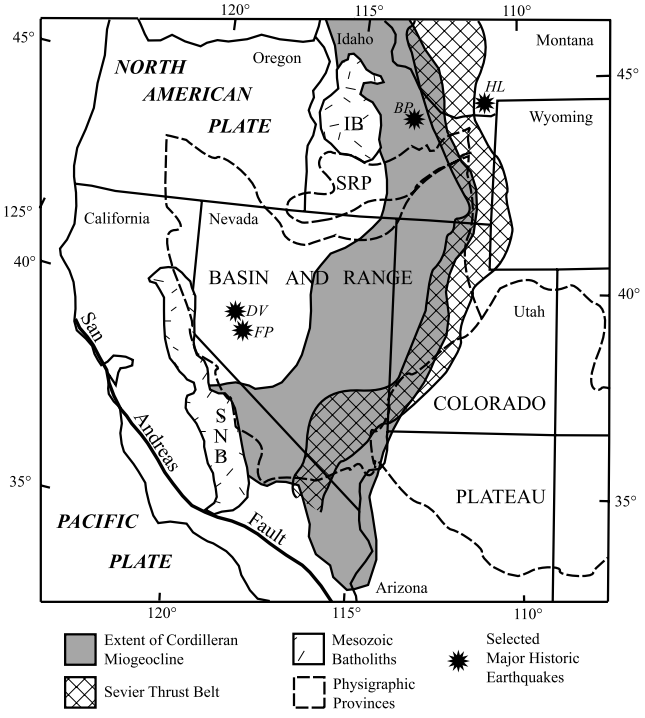

Figure 1. Map of the western USA showing major tectonic, geologic and physiographic features discussed in the text. IB, Idaho batholith; SNB, Sierra Nevada batholith. Major earthquakes discussed in the text: BP, Borah Peak; DV, Dixie Valley; FP, Fairview Peak; HL, Hebgen Lake.

a microplate description is not appropriate at any timescale (e.g. Thatcher 1995).

The predominance of one of these behaviours over the other may lie at the heart of understanding the dynamics of fault interactions. In the latter case, where deformation is evenly distributed, both spatially and temporally, conventional models of continuum behaviour of the lithosphere as a whole (e.g. England & McKenzie 1982) would be adequate for predicting the magnitude and location of interseismic strain accumulation (e.g. Bourne *et al.* 1998), but predicting the next earthquake in the system would be exceedingly difficult. In the former, seismic hazard would be highest in the region of contemporary localized strain accumulation, but would migrate from fault to fault within the system on relatively short timescales. In such a scenario, probabilistic earthquake prediction would be rather straightforward, but the migration of localized strain accumulation in the lithosphere would be ill-explained by any current dynamic and rheologic models of the Earth.

Despite considerable effort, campaign-mode geodetic surveys using triangulation, trilateration, VLBI, or Global Positioning System (GPS) techniques have failed to adequately address this question, largely because uncertainties in intersite velocities are in excess of 1–2 mm yr^{-1} (Savage *et al.* 1992; Dixon *et al.* 1995; Savage *et al.* 1996; Thatcher *et al.* 1999), greater than the horizontal displacement rates across most intraplate fault zones. To overcome this problem, we established a continuously monitored, 50-site GPS network covering the northern and central Basin and Range province (Basin and Range Geodetic Network, or BARGEN; Wernicke *et al.* 1998, 2000). The first 18 sites, in an east–west transect from central Utah to eastern California near latitude 40°N, began recording site positions in 1996 (Fig. 2; Bennett *et al.* 1998a, 1999, 2002). Results, based on the first 2 yr of data, yielded velocity uncertainties of <0.5 mm yr^{-1} (Davis *et al.* 2003) and suggested significant strain accumulation outside of the three major seismic belts. The strain field in the Basin and Range is partitioned into two components: east–west dilation averaging 3 mm yr^{-1} in the eastern portion of the province and north–northwest right-lateral shear at 9 mm yr^{-1} in the western part (Dixon *et al.* 1995; Bennett *et al.* 1998a, 1999; Wernicke *et al.* 2000; Bennett *et al.* 2003).

To fully exploit this high-precision geodetic data, we seek to place these geodetic velocities in context with geological displacement rates. Geologically determined slip rates on dip-slip faults are generally vertical displacement rates, but the highest precision GPS velocities are the horizontal rates. Therefore, comparing the two velocities requires deriving horizontal geological displacement rates from geological data, which requires knowledge of the dip of fault zones through the crust. In other words, knowing only the position of the surface traces of Basin and Range faults, vertical geological offsets and geodetic velocities is insufficient to compare the two velocity fields. This is especially true in the case of Basin and Range normal faults because their subsurface dips appear to range from subhorizontal to greater than 60° and therefore the horizontal slip rate for any given vertical rate may be uncertain by an order of magnitude if fault dip is not known.

In this paper, we illustrate an approach to investigating the dynamics of fault systems by combining geological data, including the subsurface geometry of faults and their vertical slip rates at the surface, with high-precision geodetic data. We use the BARGEN horizontal velocity field in a transect from the Colorado Plateau to central Nevada, the only region in the Basin and Range where the deep subsurface geometry of normal faults is known from seismic reflection profiling for a significant across-strike distance of the province (Figs 3 and 4; Allmendinger *et al.* 1983, 1987). We use maximum vertical fault slip rates and subsurface fault geometries to map the average late Quaternary horizontal velocity field of the seismogenic crust and then compare the geological velocity field with the geodetic velocity field, to evaluate whether strain accumulation is localized within the Intermountain seismic belt (Dixon *et al.* 1995; Martinez *et al.* 1998; Thatcher *et al.* 1999; Dixon *et al.* 2000), or distributed more evenly so as to include the broad region of late Quaternary faults to the west (Bennett *et al.* 1999).

The transect includes the very low angle Sevier Desert detachment, expressed as a band of prominent multicyclic reflections, dipping ∼10–12°W underneath the Sevier Desert from the surface to a depth of 12–15 km (Allmendinger *et al.* 1983; Planke & Smith 1991). Some geologists have suggested the reflection band is an unconformity in its shallow reaches and a Mesozoic thrust fault at depth (Anders & Christie-Blick 1994), casting doubt on whether the structure has ever had normal slip. Therefore, if significant strain accumulation is observed across the Sevier Desert region, our analysis has implications for the ability of low-angle (0–30°) normal faults to accommodate this strain.

2 TECTONIC SETTING

The baseline CAST–SMEL lies astride the Intermountain seismic belt (Figs 2 and 3), which coincides with three other major elements of the Cordilleran orogen, collectively known as the Wasatch line or Wasatch zone. These elements have defined the eastern margin of the orogen throughout most of its history, and include the hinge zone of west-thickening shallow marine sediments of Proterozoic and Palaeozoic age (Cordilleran miogeocline), the east limit of east-directed decollement thrust faulting and folding of Mesozoic age

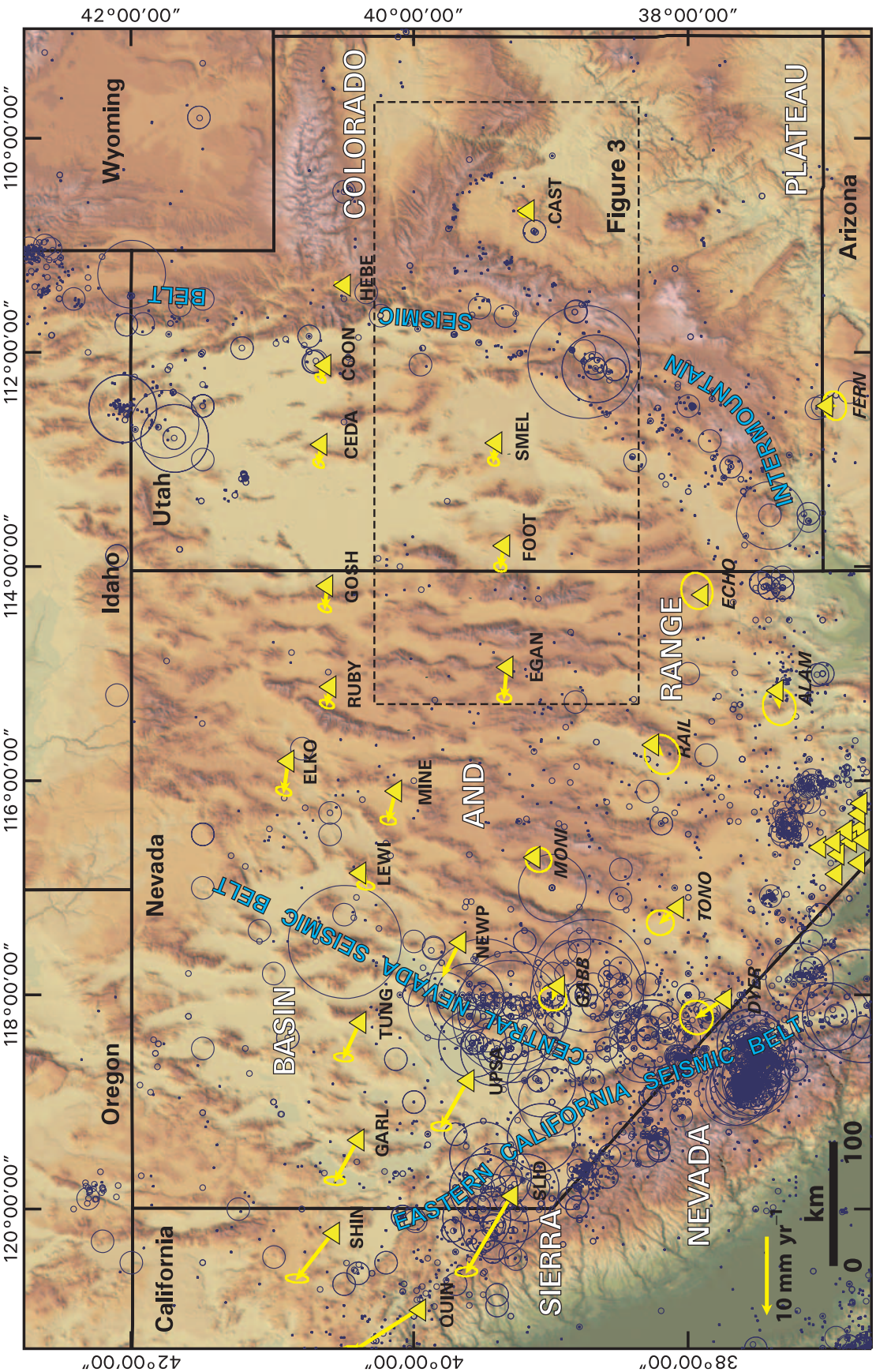

Figure 2. Shaded digital elevation model of the western USA showing the major seismic belts and earthquakes greater than magnitude 3.0 in blue circles. Yellow triangles are GPS sites of the BARGEN network; sites labelled in bold text are part of the initial BARGEN network and have been operational since 1997; sites labelled in italicized text are part of the expanded BARGEN network and have been operational since 1999. Sites near Yucca Mountain and the Nevada Test Site (~ 116° W at the bottom edge of the figure) unlabelled. Location of Fig. 3 is shown with a dashed box.

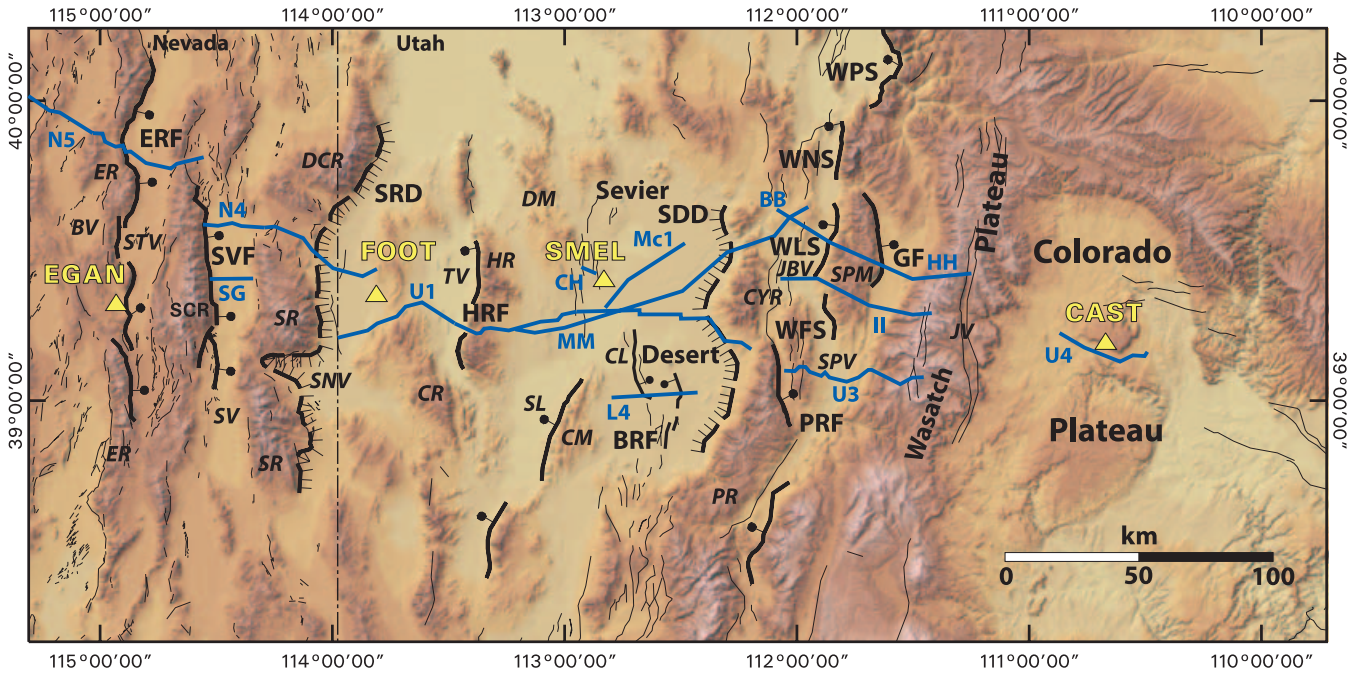

Figure 3. Shaded relief map of the area of study showing GPS sites (yellow triangles), seismic reflection profiles (blue lines) and surface traces of high-angle (bold line with ball-and-bar symbol on hangingwall) and low-angle (hachures on hangingwall) normal faults. Faults: BRF, Black Rock fault zone; ERF, Egan Range fault; GF, Gunnison fault; HRF, House Range fault; PRF, Pavant Range fault; SDD, Sevier Desert detachment; SRD, Snake Range detachment; SVF, Spring Valley fault; WFS, Wasatch fault, Fayetteville segment; WLS, Wasatch fault, Levan segment; WNS, Wasatch fault, Nephi segment; WPS, Wasatch fault, Provo segment. Lakes: CL, Clear Lake; SL, Sevier Lake. Mountain Ranges: CM, Cricket Mountains; CR, Confusion Range; CYR, Canyon Range; DCR, Deer Creek Range; DM, Drum Mountains; ER, Egan Range; HR, House Range; PR, Pavant Range; SCR, Schell Creek Range; SPM, San Pitch Mountains; SR, Snake Range. Valleys: BV, Butte Valley; JBV, Juab Valley; JV, Joes Valley; SNV, Snake Valley; SPV, San Pete Valley; STV, Steptoe Valley; SV, Spring Valley; TV, Tule Valley. Reflection profiles: CH, Drum Mountains scarps (Crone & Harding 1984); L4, seismic line 4 of Planke & Smith (1991); Mc1, seismic line 1 of McDonald (1976); MM, BB, HH, II, seismic lines MM′, BB′, HH′ and II′ of Smith & Bruhn (1984); N4 and N5, COCORP Nevada lines 4 and 5 (Hauser *et al.* 1987); SG, Spring Valley (Gans *et al.* 1985); U1, U3 and U4, COCORP Utah lines 1, 3 and 4 (Allmendinger *et al.* 1987).

(Sevier thrust belt), and the eastern limit of Cenozoic crustal extension in the Basin and Range province (Fig. 1).

West of the Wasatch zone, sites SMEL, FOOT, EGAN and MINE lie within the miogeocline, which has been variably shortened by thrust faulting in the Late Palaeozoic and Mesozoic, and extended by normal faulting in the Late Mesozoic and Cenozoic (e.g. Burchfiel *et al.* 1992). These events have been punctuated by magmatic episodes in Late Jurassic, Late Cretaceous and mid-Tertiary time, with significant Quaternary basaltic volcanism in the Sevier Desert region southeast of site SMEL (Hintze 1988).

Large-magnitude extension along regional detachment faults began in early Miocene time along the east-dipping Snake Range detachment and associated faults to the west (Lee 1995; Lewis *et al.* 1999; Miller *et al.* 1999) and in late Oligocene or early Miocene along the west-dipping Sevier Desert detachment to the east (Fig. 3; Allmendinger *et al.* 1983; Von Tish *et al.* 1985; Allmendinger & Royse 1995; Otton 1995; Stockli *et al.* 2001).

The overall asymmetry of the early extensional faulting is maintained in the structure of the modern range-bounding fault zones. Faults along the eastern half of the transect, including the Wasatch, Sevier Desert and House Range faults, dip predominantly to the west, and those along the western half of the transect, including the Snake Range, Spring Valley and Egan Range faults, dip to the east (Figs 3 and 4).

3 METHODS AND ASSUMPTIONS

3.1 GPS data

GPS site velocities were determined using daily GPS position estimates for a worldwide network of GPS stations, including BARGEN sites, from 1997 February to 2000 April (Fig. 2). At each BARGEN site, GPS antennas are mounted on Wyatt-type monuments, generally considered the most stable type of geodetic monument (Wyatt 1982; Langbein *et al.* 1995; Wernicke *et al.* 1998, 2000). GPS phase measurements are recorded every 30 s, and the sites are downloaded daily. These data are processed, using the GAMIT/GLOBK software (Herring 1999; King & Bock 1999), to yield a network velocity solution in a global reference frame that includes several hundred sites in addition to the BARGEN sites, following procedures described in Bennett *et al.* (1999, 2002). Daily horizontal position estimates are repeatable at the 1–2 mm level. Velocity solutions for the first 3 yr of BARGEN data yield formal errors in velocity of 0.1–0.2 mm yr^{-1} (Bennett *et al.* 1999; Davis *et al.* 2003).

These formal errors, which are based on uncertainties in receiver timing, phase measurement, satellite position, Earth orientation, atmospheric effects and other factors, may underestimate the true errors in velocity and position because monument stability (e.g. Langbein & Johnson 1995) and other sources of error are not modelled. Observed scatter about a line regressed through the west velocity components of all the BARGEN sites is 0.5 mm yr^{-1}. Because the

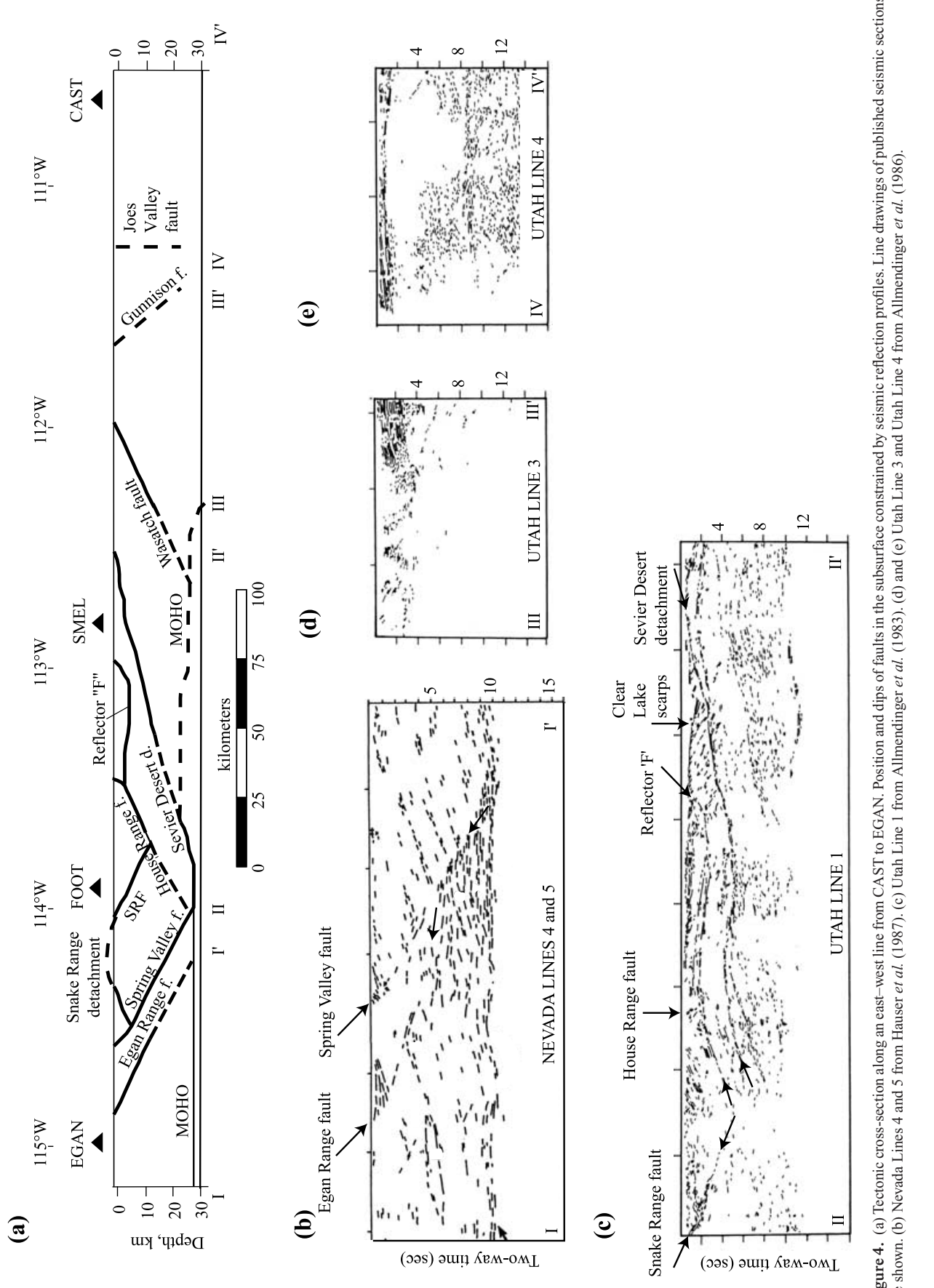

Figure 4. (a) Tectonic cross-section along an east–west line from CAST to EGAN. Position and dips of faults in the subsurface constrained by seismic reflection profiles. Line drawings of published seismic sections are shown. (b) Nevada Lines 4 and 5 from Hauser *et al.* (1987). (c) Utah Line 1 from Allmendinger *et al.* (1983). (d) and (e) Utah Line 3 and Utah Line 4 from Allmendinger *et al.* (1986).

observed scatter encompasses uncertainty resulting from both modelled and unmodelled sources of error, as discussed above, as well as actual variations in intersite velocities, a much larger observed scatter would be expected if the true errors in measurement substantially exceeded the formal errors (Davis *et al.* 2003). Conservatively, we will assume a maximum error in velocity at each site of 0.5 mm yr^{-1}, while noting that true errors may actually be as low as the formal errors (Davis *et al.* 2003).

3.2 Seismic reflection data

Subsurface fault geometries were obtained from published structural interpretations of seismic reflection profiles shot normal to the traces of major normal faults (Figs 3 and 4). There may be considerable uncertainty in fault dip for any given plane imaged on reflection profiles as a result of migration, uncertainties in velocity and 3-D effects such as out-of-plane reflections. For faults under consideration here, most of which are imaged throughout a substantial thickness of the crust, uncertainties in fault position and dip are less than a few kilometres and a few degrees, respectively (e.g. McDonald 1976; Allmendinger *et al.* 1983; Smith & Bruhn 1984; Gans *et al.* 1985; Allmendinger *et al.* 1987; Hauser *et al.* 1987; Planke & Smith 1991; Coogan & DeCelles 1996).

3.3 Palaeoseismological data

In addition to the constraints on horizontal motions from geodesy, we use vertical offsets, or net vertical tectonic displacements (NVTDs, Fig. 5; Witkind 1964; Crone *et al.* 1987; Caskey 1996) recorded across Basin and Range fault scarps, to estimate the horizontal displacement rate of the seismogenic layer accommodated along the faults, averaged over some fraction of late Quaternary or Neogene time. Except for the Wasatch fault, these rates are generally known only to within an order of magnitude. In general, the minimum slip rates for most structures are effectively zero ($\ll$0.1 mm yr^{-1}) and

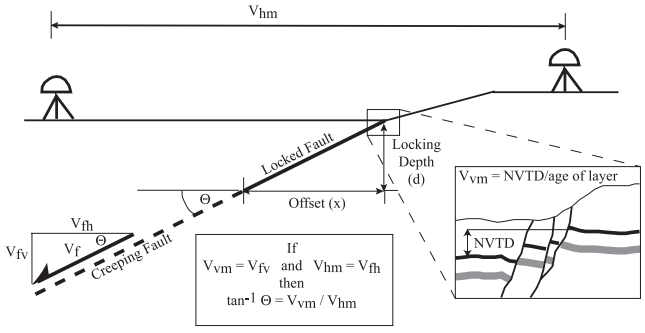

Figure 5. Schematic diagram showing relationship of horizontal and vertical velocity components of coseismic slip on faults with horizontal GPS velocities and fault dips. Cross-section is not intended to be to scale. If a pair of GPS sites measure the far-field horizontal strain across a fault, then the horizontal coseismic strain release on that fault should equal the average geodetic velocity multiplied by the coseismic recurrence interval, if all of the accumulated strain is released seismically. Additionally, the vertical component of slip on the fault should be related to the horizontal component through the tangent of the fault dip. Given that these assumptions are true, vertical slip rates determined from palaeoseismology can be related to horizontal GPS velocities. Cartoon of NVTD measurement is representative of palaeoseismological methods used to determine vertical slip rates on active faults; however, a wide variety of methods are used to constrain vertical slip rates (Table 1, Appendix A).

therefore their sum will contribute little to the geological velocity field. The more interesting question is whether the maxima, which can be fairly well established (Table 1), sum to equal the geodetic rate.

Even to within an order of magnitude, we would not necessarily expect vertical slip rate estimates to agree with those based on fault dip and horizontal motion, for several reasons. The first is that the time intervals sampled for geological and geodetic data differ by as much as 6 orders of magnitude. Non-linear strain accumulation along or near seismogenic faults is common in the interval following large earthquakes, where strain rates may be a factor of 2–3 higher than the interseismic average (e.g. Thatcher 1983; Wernicke *et al.* 2000). However, these strain transients appear to have decay times of the order of years to decades, not centuries, and are thought to result mainly from either stable sliding in unconsolidated materials near the surface of the Earth, or viscous relaxation near the base of the seismogenic part of the crust (e.g. Savage & Prescott 1978; Scholz 1990; Hager *et al.* 1999). In general, however, geologically determined slip rates appear to be in agreement with slip rates modelled geodetically in the interseismic period, at least for major plate boundary fault zones where the two sets of data may be compared (e.g. Thatcher 1990; Bennett *et al.* 1996; Ward 1998). In addition, there is remarkably good agreement between geodetic and plate tectonic estimates of relative plate motion, despite the contrast in sampling interval of 5 orders of magnitude (Ma *et al.* 1993; Larson *et al.* 1997). Because there have not been any earthquakes in our study region that have ruptured most or all of the seismogenic layer during at least the last 500 yr (Hecker 1993; McCalpin *et al.* 1996), there is no phenomenological basis, at least at present, to expect contemporary motions to differ from those averaged over late Quaternary time.

The second reason one might not expect geological and geodetic determinations of fault slip rates to agree relates to the problem of curviplanar or listric faults, wherein the vertical offset along the steep, upper crustal portion of the fault may significantly exceed the vertical component of motion on the more shallowly dipping subsurface trace (Verrall 1981; Wernicke & Burchfiel 1982; White *et al.* 1986; Jackson 1987). In general this must be accounted for on a fault-by-fault basis, but so long as the deflection from steeper dip to shallower dip is relatively modest ($<$20–30°) and geological slip estimates carefully differentiate between the total height of the fault scarp and the NVTD accommodated by the fault, we would not expect a significant contrast between vertical slip rates at depth and at the surface (Fig. 5).

Lastly, surface vertical offsets may underestimate offsets at depth to the extent that surface deformation is accommodated by long-wavelength flexure or penetrative strain that may be difficult to detect using palaeoseismological methods (Thatcher & Bonilla 1989; Caskey 1996). This is commonly the case for thrust or reverse faults, where upper crustal layers, especially sediments, buckle in compression instead of fracturing, resulting in a blind fault geometry (e.g. Schneider *et al.* 1996). Normal faults, on the other hand, typically fracture surficial layers. In the cases where data are available, the NVTDs on normal fault scarps are in good agreement with wide-aperture geodetic measurement of coseismic vertical motion (Table 2). Within error ($\sim$10 to 50 per cent), they also agree with estimates of the vertical component of mean fault slip at depth derived from inversion of geodetic and seismic data (Table 2). This is noteworthy in that we would not generally expect surface displacements for individual earthquakes to reflect the pattern of slip at depth. For a series of earthquakes on the same fault zone, then, the NVTD rate should reflect the vertical component of fault slip at depth for

Table 1. Estimated maximum vertical fault-slip rates for faults in west-central Utah and eastern Nevada.

Fault or fault segment	Timescale				
	Historic 10^2 yr	Holocene 10^3 yr	Latest Pleistocene 10^4 yr	Late to mid-Pleistocene 10^5 yr	Plio–Miocene 10^6–10^7 yr
Wasatch					
Nephi	$1.9^{a}_{1,2}$	$\mathbf{1.3}^{b,d}_{1,2,3}$	$\mathbf{0.3}^{d}_{3}$	$\mathbf{0.2}^{e}_{1}$	
Levan	$2.0^{a}_{2,4}$	0.4^{c}_{2}			
Fayette		$0.2^{a,h}_{1}$			
Gunnison		Late Holocene$_3$			
Pavant Range		Late Holocene$_3$			
Sevier Desert					
Black Rock	2.0^{e}_{6}	1.4^{e}_{6}	0.2^{e}_{6}	0.1^{e}_{6}	
Clear Lake		$\mathbf{0.3}^{e}_{7,8}$			$\mathbf{0.2}^{i}_{9}$
Drum Mountains		0.4^{a}_{10}	$\mathbf{0.4}^{i}_{7}$		0.2^{d}_{8}
House Range		$0.2^{e}_{5,11,12}$			$\mathbf{0.2}^{k}_{13}$
Spring Valley		$0.1^{e}_{14,15}$	$\mathbf{0.3}^{h}_{16}$	$\mathbf{0.1}^{g}_{17}$	0.3^{j}_{18}
Egan Range				$0.1^{e,g}_{12,15,17}$	0.1^{j}_{18}

Note: maximum vertical slip rates calculated for each order of magnitude timescale. Boldface slip rates are better constrained and considered most robust (for discussion, see Appendix A).

Palaeoseismological methods

[a]The vertical slip rate was calculated based on the net vertical tectonic displacement (NVTD) of the most recent event (MRE) in a trench. The MRE is constrained by the youngest faulted deposit and the oldest unfaulted deposit, but this age may not be closely limiting (e.g. McCalpin & Nishenko 1996).

[b]The vertical slip rate was calculated by linear regression through the rates of multiple events exposed in a trench, but not extrapolated to the present day.

[c]The vertical slip rate since the penultimate event (PUE) is constrained by the oldest unfaulted deposit not related to the MRE and by assuming an NVTD similar to the MRE.

Geomorphic methods

[d]Non-linear scarp-diffusion profile models were used to determine the age of the deposit and the offset from which slip rates are calculated (Mattson & Bruhn 2001).

[e]The vertical fault slip rate is based on the offset of alluvial fans, shorelines, or basalt flows of known age (e.g. Machette *et al.* 1992a). Typically, only one age datum, so that the calculated slip rate has to be extrapolated to the present day.

[f]The slip rate is based on the age of the alluvial fan cut by a fault, but faulting may be significantly younger than the age of the fan, and the age of the faulted strata are not closely limiting (e.g. McCalpin & Nishenko 1996).

[g]The slip rate has been determined empirically by dePolo (1998) based on a relationship between slip rate and facet height. The lack of active fault facets along the range front implies a maximum fault slip of 0.1 mm yr^{-1} (dePolo 1998).

[h]The fault-scarp age is determined empirically by comparison of scarp height and slope angle with calibrated fault scarps (e.g. Bucknam & Anderson 1979a).

Structural and seismic reflection data

[i]The vertical slip rate is based on marker units offset across the fault, visible in seismic reflection profiles; the age of the offset marker is known from drill hole data.

[j]The maximum fault offset is estimated from seismic reflection profiles (basin geometry and fill); the approximate age of basin fill is known from well data.

Thermochronology

[k]Apatite fission-track length modelling (Stockli *et al.* 2001). Fission-track data are obtained for an exhumed crustal section and converted to a vertical exhumation rate by assuming a geothermal gradient.

References

[1]Machette *et al.* (1992a); [2]Jackson (1991); [3]Mattson & Bruhn (2001); [4]Schwartz & Coppersmith (1984); [5]Hecker (1993); [6]Hoover (1974); [7]Oviatt (1989); [8]Crone & Harding (1984); [9]Von Tish *et al.* (1985); [10]Crone (1983); [11]Piekarski (1980); [12]Ertec Western, Inc. (1981); [13]Stockli *et al.* (2001); [14]Friedrich (unpublished data); [15]Dohrenwend *et al.* (1992); [16]Haller & Machette (unpublished data); [17]dePolo (1998); [18]Gans *et al.* (1985).

relatively planar normal faults, providing that the rupture propagates to the surface.

The NVTD for fault scarps may be estimated over a broad range of timescales, from those involving only the most recent earthquakes, to those based on offset markers that are millions of years old, including the unroofing of isotherms as constrained by mineral cooling ages (Table 1). The ages of offset markers are not tightly constrained for most of the faults studied across our transect, making our objective to only conservatively estimate an upper limit to the vertical slip rate on each fault in late Quaternary time. For some faults (e.g. the Wasatch) these estimates are obtained by determining the average rate of slip based on the timing and offset of the last 2–3 earthquakes, which give relatively accurate NTVD rates over the last $\sim$ 5–10 ka (Table 1). For others, maximum rates are derived via net offsets of

Table 2. Coseismic vertical displacements for selected historic normal fault earthquakes.

Date	M_w	Location	Average dip of rupture plane	Surface Displacement			Subsurface Displacement	
				Maximum NVTD[a] (m)	Average of five largest NVTDs (m)	Geodetic measurement[b] (m)	Average dip-slip (m)	Vertical component of dip-slip (m)
1983	7.3	Borah Peak	50°	2.7[1]	2.3[1]	>1.7[2]	2.1–2.2[2]	1.6–1.7
1981	6.4	Gulf of Corinth	50°	1.8[7]	1.0[7]	>0.8[8]	1.0–2.2[8]	0.8–1.7
1959	7.3	Hebgen Lake	65°	5.5[3,4]	4.8[3,4]	6.4[3,4]	6.5–11.8[2]	5.6–10.1
1954	7.2	Fairview Peak	60°	3.8[5]	3.1[5]	—	1.8[6]	∼1.5
1954	7.3	Dixie Valley	50°	2.8[5]	2.5[5]	—	3.6[6]	∼2.8

[a]Net vertical tectonic displacement (NVTD).
[b]From levelling or shoreline submergence data.
[1]Crone *et al.* (1987); [2]Barrientos *et al.* (1987); [3]Witkind (1964); [4]Myers & Hamilton (1964); [5]Caskey (1996); [6]Hodgkinson *et al.* (1996); [7]Jackson *et al.* (1982); [8]Hubert *et al.* (1996).

relatively old geomorphic surfaces tens or hundreds of thousands of years old, wherein we assume the youngest possible age of the surface to estimate maximum slip rates (Table 1). Therefore, in our analysis we use the upper limit of vertical slip rate to estimate the maximum horizontal component of slip at depth, converted using the average dip of the fault derived from seismic reflection data.

3.4 Strain accumulation models

A wide variety of models have been proposed that relate strain along the locked, seismogenic parts of fault zones and strain patterns at depth. One of the most commonly used models assumes aseismic creep along the downdip segments of fault zones (e.g. Savage & Hastie 1966; Eyidogan & Jackson 1985; Bruhn & Schultz 1996). However, are these models, which predict elastic strain resulting from slip on buried edge dislocations, applicable to interseismic deformation on continental normal faults?

The simplest model for dip-slip faults assumes an infinitely long (2-D) edge dislocation that projects downwards from some locking depth to infinity (e.g. Savage 1980, 1983; Thatcher *et al.* 1999). In this model, the far-field components of surface displacement result from slip on portions of the dislocation at great distances along strike and at depth from the seismogenic portion of the fault.

In the northern Basin and Range province, however, faults are of limited strike length, from ∼30 to 70 km long for individual segments (e.g. Machette *et al.* 1991), with the total along-strike length of the active region ∼500 km (Fig. 2). Furthermore, the faults probably do not project downwards significantly below the seismogenic crust (broadly, 10–20 km thick). Most workers believe the fault blocks rest on a relatively weak substrate (e.g. Stewart 1978), which is unlikely to support significant elastic stresses on the millennial timescale of the Basin and Range seismic cycle. Therefore, even for a locking depth as shallow as 10 km (the lower depth limit of 95 per cent of earthquakes in the transect area; Lowry & Smith 1995), the downdip extent of the faults below the locking depth is unlikely to exceed 20 km (say, a 30° fault from 10 to 20 km depth).

The effect of the finite size of potentially creeping fault segments at depth on surface velocities, versus that of infinite faults, is significant. This is illustrated in Fig. 6 for a 30° fault that is locked through the seismogenic portion of the crust, say the upper 10 km. Below this depth, the fault creeps at a rate of 1 mm yr^{-1} (fault parallel). By restricting the depth of slip from infinity to a finite interval between 10 and 20 km depth, far-field surface velocities (aperature of ∼200 km) are reduced from 0.8 to 0.05 mm yr^{-1}. For the same fault with the along-strike dimension reduced from infinity to

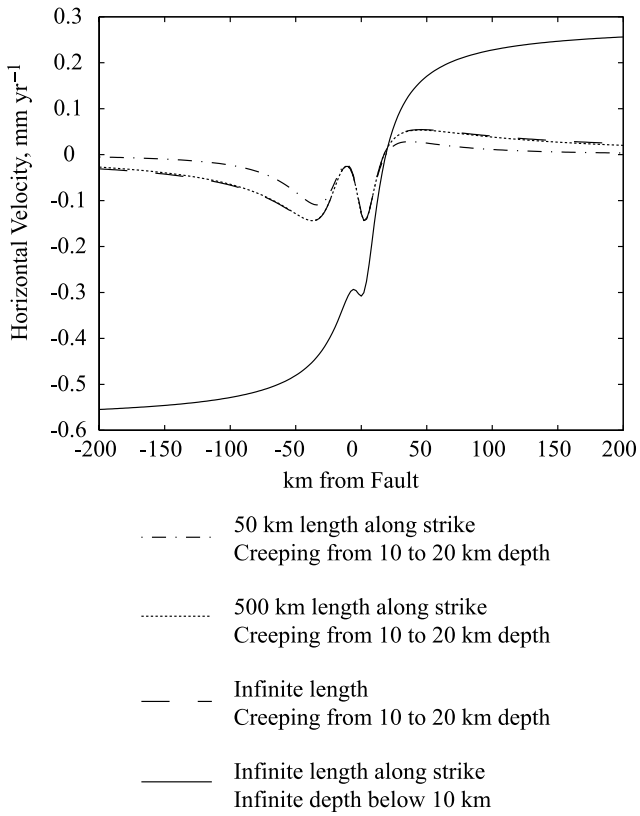

Figure 6. Comparison of displacements from elastic dislocation models for dip-slip faults of infinite and finite dimensions (Okada 1985). The along-strike length of the dislocation was varied from infinity to 50 km and the down-dip extent from infinity to 20 km. In all models, the dislocation dips 30°, is locked from the surface to 10 km depth and creeps at 1 mm yr^{-1}. Note that reducing the down-dip extent of the dislocation from infinity to 20 km reduces the amount of horizontal displacement by ∼90 per cent. Shortening the along-strike length from infinity to 50 km reduces the horizontal displacement by ∼20 per cent.

50 km, the far-field velocity is effectively zero. With either infinite or finite along-strike length, the total near-field anomaly is <0.1 mm yr^{-1} for each millimetre per year of fault slip.

Clearly, the far-field velocity field in these models is generated by portions of the dislocations that are unlikely to exist beneath the Basin and Range, while those portions that do exist and may be creeping do not contribute significantly to the velocity field. It

therefore seems inappropriate to model the velocity field of the Basin and Range using simple elastic dislocation models.

Alternative dislocation models to that discussed above have been proposed to avoid infinite edge dislocations (e.g. Matsu'ura *et al.* 1986). These models can be categorized as block models; geodetic stations are used to define the velocities of stable blocks relative to one another and the discrepancy between velocities between adjacent blocks is assumed to represent slip on a finite dislocation between the blocks. This type of model works well for near-vertical strike-slip faults, where all fault motions are horizontal (Matsu'ura *et al.* 1986), however modelling dislocations in this manner becomes more complicated with dip-slip faults. To account for horizontal motions between two blocks separated by a dipping dislocation, either vertical motions must be allowed between the two blocks, or the dislocation must open, in the case of a normal fault, or close, in the case of a thrust fault, perpendicular to the dislocation, to eliminate vertical motion. Because we do not have the necessary geodetic data to constrain vertical motions between blocks, nor in this particular case do we have the requisite GPS station density to constrain even horizontal motions between all of the mountain ranges in the study area, a block style dislocation model is also inappropriate for our purposes.

We will assume, then, that far-field components in the velocity field result from simple elongation (pure shear) of the seismogenic layer above an extending substrate, that strain in the seismogenic crust is solely a result of this elongation and that this strain is released through seismic events on the faults observed through seismic reflection profiling along the transect. Horizontal geodetic velocities would therefore measure the strain accumulated in the crust by this shear and should be equivalent to the sum of the average horizontal slip rates on the observed faults.

4 FAULT GEOMETRY AND LATE QUATERNARY VERTICAL SLIP RATES

4.1 Wasatch and related faults

The Wasatch fault zone, perhaps the best-studied normal fault in the world, is approximately 350 km long and divisible into 10 segments (Machette *et al.* 1991, 1992b). The baseline CAST–SMEL encompasses the three southernmost segments, including, from north to south, the Nephi, Levan and Fayette segments, which define the western boundary of the Wasatch Range and San Pitch Mountains (Figs 3 and 4; Machette *et al.* 1991, 1992b). In addition to the Wasatch fault zone, two east-dipping fault segments, the Gunnison and Pavant Range faults (Hecker 1993) cross this baseline. The Pavant Range fault defines the steep northeast margin of the Pavant Range and appears to represent a major right-step in the Wasatch system (Fig. 3), forming a low-relief accommodation zone (Rosendahl 1987). The Gunnison fault lies along the east flank of the San Pitch Mountains and, with the Levan segment, defines the northern San Pitch Mountains as a structural horst (Fig. 3). These five fault segments all have late Quaternary (<130 ka) slip, including multiple Holocene (<10 ka) offsets along the Levan and Nephi segments (Table 1).

To the east of these faults, on the Colorado Plateau, zones of Holocene faulting define two narrow grabens, the most prominent forming the narrow Joes Valley (Figs 3 and 4a). These faults do not define a major range block and are generally believed to accommodate collapse of post-Jurassic strata as a result of the westward flow of Jurassic evaporites toward the Basin and Range (Hecker 1993), and hence it is unlikely that they penetrate pre-Jurassic strata as significant faults.

For the Wasatch fault, dips in outcrop range from 35° to 70° (e.g. Bruhn *et al.* 1992). The subsurface configuration of the range-bounding structures, however, is not well known in the transect area, except for a reflection profile indicating that a portion of the Levan segment dips 34°W at 2 km depth (Fig. 4a; Smith & Bruhn 1984). Seismic reflection profiles and well data across the Sanpete Valley indicate continuity of pre-Middle Jurassic (pre-Arapien shale) strata between the San Pitch Mountains and the Wasatch Plateau, suggesting that the Gunnison fault soles into the Arapien at a depth of less than 4 km (Standlee 1982).

Palaeoseismological data for the Levan and Nephi segments indicate maximum late Holocene (<3 ka) vertical displacement rates of 2.0 and 1.9 mm yr^{-1}, respectively, by simply extrapolating from the most recent earthquake to the present (Table 1). This is probably a gross overestimate (Appendix A). Where best constrained, on the Nephi segment, three events with a total NVTD of <7 m have occurred since >4.8 ka, yielding a maximum vertical rate of 1.3 mm yr^{-1} (Appendix A). On the Nephi segment, a 30-m offset of a fan surface no younger than ∼150 ka suggests a long-term vertical rate no greater than 0.2 mm yr^{-1} and scarp diffusion modelling suggests vertical rates of ∼0.3 mm yr^{-1} from 35 to 70 ka (Table 1; Appendix A). On the Levan segment, two events since 7.3 ka yield a vertical rate of only 0.4 mm yr^{-1}.

4.2 Sevier Desert detachment and related faults

The Sevier Desert reflection, which has been interpreted as a low-angle detachment fault, is a band of prominent multicyclic reflections that dip 12° westwards and can be traced continuously in seismic sections from depths of 12 to 15 km to their surface projection along the western margins of the Canyon and Pavant ranges (Figs 3, 4a and c; Allmendinger *et al.* 1983; Planke & Smith 1991).

Anders & Christie-Blick (1994) have challenged this interpretation, based on an analysis of microfracture density of well cuttings recovered from a borehole that penetrates the reflection just west of the Pavant Range. They concluded that the densities were lower than expected for a damage zone adjacent to a fault, and proposed that the reflection represents an unconformity between Miocene and Cambrian strata, rather than a fault. Their hypothesis is not generally accepted (e.g. Allmendinger & Royse 1995; Otton 1995; Wernicke 1995; Coogan & DeCelles 1996) because: (i) a major exposed detachment fault (Cave Canyon detachment) projects beneath the Sevier Desert Basin along its south flank (Coleman & Walker 1994; Coleman *et al.* 1997); (ii) rocks beneath the reflection yield Miocene cooling ages, while the basin began subsiding in the Oligocene (Von Tish *et al.* 1985; Allmendinger & Royse 1995; Stockli *et al.* 2001); and (iii) the overall reflection geometry is strongly analogous to exposed detachment systems throughout the Basin and Range (Wernicke 1981; Allmendinger *et al.* 1983; Anderson 1983; Smith & Bruhn 1984; Allmendinger *et al.* 1987; Planke & Smith 1991; Otton 1995; Wernicke 1995; Coogan & DeCelles 1996). Hence, for the purposes of our analysis, we will consider only the possibility that the reflections represent a detachment fault, which may be an active structure.

A number of high-angle fault zones either sole into, or are truncated by, the Sevier Desert detachment (McDonald 1976; Planke & Smith 1991; Coogan & DeCelles 1996). The two most extensive of these fault systems are an antithetic (east-dipping) fault zone running down the centre of the Sevier Desert Basin (Western Basin-Bounding fault of Planke & Smith 1991) and a west-dipping

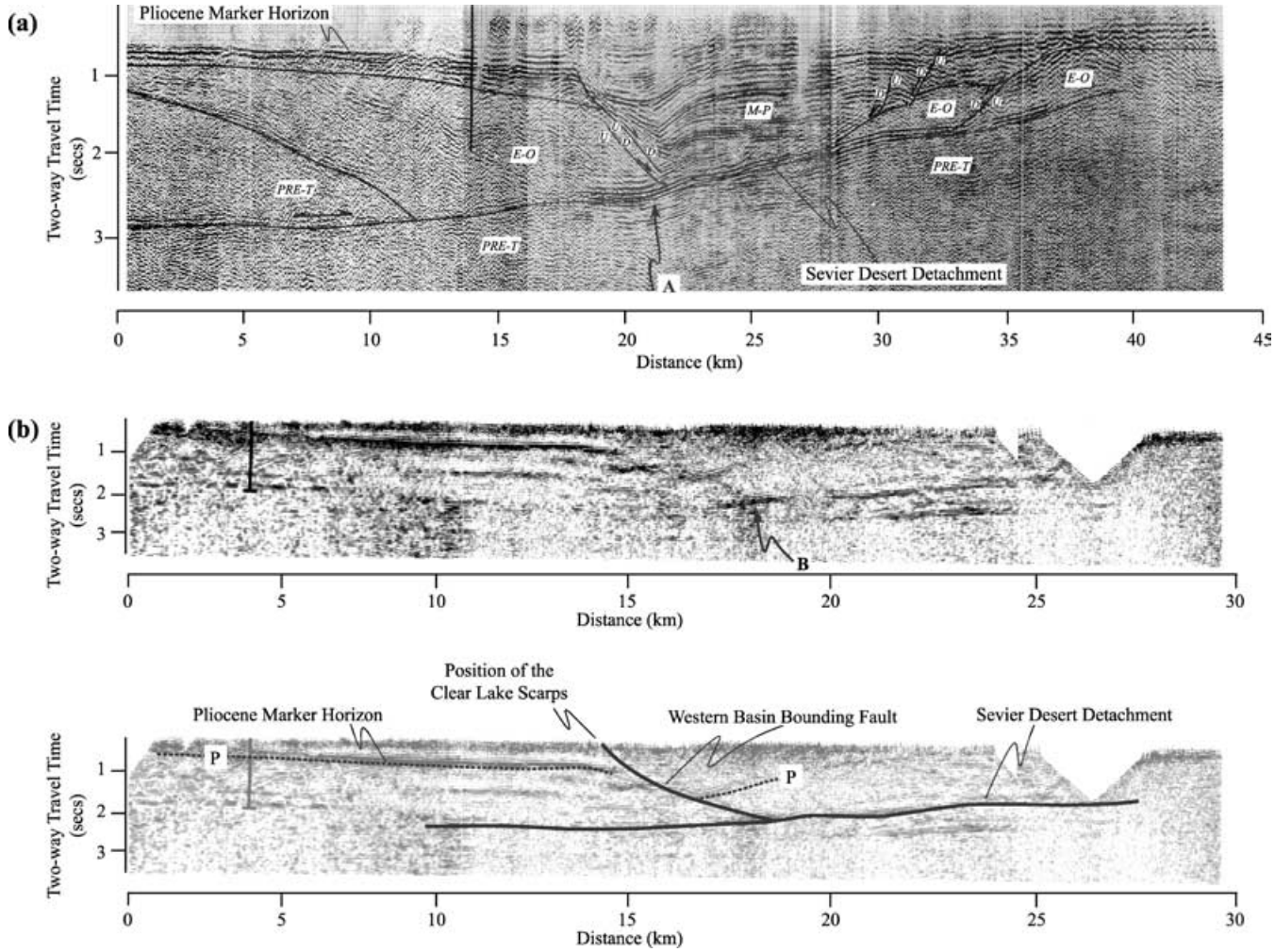

Figure 7. Seismic reflection lines across the Sevier Desert at latitude ∼39°00′N (Fig. 3). (a) Seismic reflection line across the central Sevier Desert Basin, modified after line 1 (plate 1) of McDonald (1976). McDonald interprets the west-dipping fault bounding a Miocene–Pliocene growth basin to truncate downwards against the detachment plane (at point A). (b) Uninterpreted and interpreted seismic reflection lines showing the position of the Clear Lake scarps (Oviatt 1989) with respect to the Western Basin-Bounding fault (WBBF), after fig. 4 (line 4) of Planke & Smith (1991). They interpret the fault to offset a brightly reflective sequence of Pliocene basalts (horizon P on interpreted section) > 1000 m, with the fault plane reflections merging with the detachment without offsetting it (at point B on uninterpreted section). Similar relations between the WBBF and detachment are documented on lines 2, 3 and 20 of McDonald (1976), lines 2 and 10 of Planke & Smith (1991) and line GSI-15 of Coogan & DeCelles (1996).

fault zone running down the eastern edge. Although these fault zones have little topographic expression, they appear in east–west reflection profiles at approximately 112.7°W longitude (10–15 km east of SMEL), for a total along-strike distance of at least 70 km (McDonald 1976; Planke & Smith 1991). The fault zones merge southwards, such that they appear to define the margins of a north-trending graben that widens northwards under the Sevier Desert Basin. The eastern margin of the graben is defined by the Black Rock fault zone, dominated by the west-dipping Devil's Kitchen fault, which also shows evidence of Holocene offset (Condie & Barsky 1972; Hoover 1974).

4.3 Clear Lake scarps

The Western Basin-Bounding fault projects upward to coincide precisely with the Clear Lake scarps, a 30 km-long zone of both east- and west-down Holocene scarps (Figs 3 and 7; Oviatt 1989). At depth, the fault offsets a 4.2-Ma basalt horizon approximately 1000 m (Fig. 7), yielding an average mid-Pliocene to Recent vertical rate of ∼0.2 mm yr^{-1}. The most prominent of the Clear Lake scarps has a west-side-down NVTD of 3 m that is probably entirely post-Bonneville (<17 ka) and may be entirely Holocene (Oviatt 1989), suggesting a maximum vertical slip rate of ∼0.3 mm yr^{-1} (Table 1). There is clearly no equivalent vertical offset of the underlying detachment (Fig. 7; Planke & Smith 1991). Although it is possible that the recent movements responsible for the Clear Lake scarps occurred on a fault that offsets the detachment a small amount (and is therefore not detectible in the seismic reflection data), it appears far more likely that the scarps represent continued movement on the same structure that offsets the basalts. Because it is difficult to envisage how the relatively large offset on the Western Basin-Bounding fault could occur without slip on the detachment, the Clear Lake scarps strongly imply that the detachment is also active (Wernicke 1981; Crone & Harding 1984). However, it is unclear how vertical slip rates on an antithetic fault that soles into the detachment relate to the slip rate on the detachment at depth.

4.4 Black Rock fault zone

The Black Rock fault zone extends southwards from Pavant Butte some 70 km (Fig. 3; Hoover 1974) and is composed of multiple fault strands (Condie & Barsky 1972). The fault zone is developed predominantly in Quaternary basalts, thus providing some of the best constraints on the kinematics of late Quaternary faulting along our transect (Hoover 1974). The largest offset, 67 m, was measured in the 918-ka Beaver Ridge lava field, yielding an average Quaternary slip rate of ∼0.1 mm yr^{-1}. An 18.3-m offset was observed for the 128-ka Pavant volcanic field, on a fault scarp that does not offset Lake Bonneville (∼17 ka) shorelines, indicating a slip rate of ∼0.2 mm yr^{-1} over the last ∼100 ka. A 15.2-m offset across a fault scarp in the basalts of the 11-ka Tabernacle volcanic field yields a Holocene vertical slip rate of 1.4 mm yr^{-1}. A 6.1-m offset is observed in the youngest lava field in the region, the Ice Springs eruptive centre. The Ice Springs field has not been dated radiometrically, but stratigraphic evidence suggests that it is 3–4 ka, yielding a maximum late Holocene vertical slip rate of ∼2.0 mm yr^{-1} (Hoover 1974).

4.5 House Range fault and Drum Mountains scarps

The westernmost major west-dipping structure, the House Range fault, defines the steep western escarpment of the House Range and has significant late Quaternary slip (Fig. 3; Hecker 1993). The fault runs subparallel to the eastern flank of a regional antiform in Palaeozoic miogeoclinal strata imaged in reflection profiles, merging at depth either along or parallel to a major decollement thrust fault that duplicates the section (Fig. 4c; Allmendinger *et al.* 1983). Regardless of its exact position relative to the thrust, the dip of upper crustal layering on the west flank of the antiform is only ∼20–30°, and the continuity of the reflections beneath the House Range and adjacent valley precludes the range front fault from having a dip substantially different from the layering through the upper crust (Figs 4a and c; Allmendinger *et al.* 1983). Bonneville deposits with an NVTD of up to 2.5 m were offset prior to 12 ka, suggesting a maximum late Quaternary vertical rate near 0.25 mm yr^{-1} (Table 1).

Beneath and east of the House Range, a subhorizontal splay of the House Range fault runs along the crest of the antiform, steepening upwards and forming a small half graben in the vicinity of SMEL, involving only the upper 4–5 km of the crust (Figs 4a and c; reflection F of Allmendinger *et al.* 1983). The half graben underlies the Drum Mountains scarps, a system of both east- and west-dipping Holocene fault scarps that cut fan deposits along the western margin of the Sevier Desert Basin, just east of the Drum Mountains (Fig. 3; Crone & Harding 1984; Hecker 1993). As in the case of the House Range fault, these faults cannot project steeply downwards with significant offset because of the continuity of reflections in Palaeozoic strata in the shallow crust beneath them (Fig. 4c). An NVTD of not more than 7 m since 18 ka yields a late Quaternary vertical rate of 0.4 mm yr^{-1} (Table 1). The maximum late Quaternary vertical slip rate of the House Range fault at depth, west of its junction with reflection F, is presumably the sum of motion on the Drum Mountains and House Range scarps, or approximately 0.65 mm yr^{-1}.

4.6 Snake Range detachment

East-dipping structures in the transect include the Snake Range detachment (Misch 1960), the Spring Valley fault (Gans *et al.* 1985) and the Egan Range fault (Figs 3 and 4a). The subsurface projection of the Snake Range detachment is imaged west of the Snake Range beneath Snake Valley, dipping approximately 30°E through most of the upper crust, where it is interpreted to be truncated by west-dipping reflections parallel to the House Range fault (Allmendinger *et al.* 1983). Although several relatively short Quaternary scarps are present in Snake Valley, they do not define the eastern margin of the Snake Range, nor could they significantly offset the detachment at depth. Thus it appears that the Snake Valley scarps join a still-active reach of the detachment at depth that today functions as an antithetic, hangingwall splay of the House Range fault (Fig. 4). Its late Quaternary slip rate is not known.

4.7 Spring Valley and Egan Range faults

In contrast to the Snake Range, the eastern flanks of the Schell Creek Range and the Egan Range are defined by major late Quaternary fault scarps (Fig. 3; Dohrenwend *et al.* 1996). The Schell Creek Range is one of the most impressive range fronts in the Basin and Range, with net relief comparable to that of the Wasatch Range. The range-bounding fault of the Schell Creek Range, the Spring Valley fault, is well imaged in the subsurface, where it dips approximately 30° east to a depth of at least 20 km and perhaps through nearly the entire thickness of the crust (30 km), where its projection appears to truncate in a zone of bright subhorizontal reflections in its footwall near the base of the crust (Figs 4a and b; Hauser *et al.* 1987). The Snake Range detachment, which was active principally in Oligocene to middle Miocene time (Lee 1995; Miller *et al.* 1999), is cut and offset ∼6 km by the Spring Valley fault (Bartley & Wernicke 1984; Gans *et al.* 1985). The Egan Range fault is also well defined both at the surface and in the subsurface to mid-crustal depths, where it dips approximately 30° (Hauser *et al.* 1987).

With the exception of a piedmont segment along the southern trace of the Spring Valley fault, none of the faults in east-central Nevada appear to have Holocene offset and the Egan Range fault does not even appear to have been active in the late Quaternary (since 130 ka; Dohrenwend *et al.* 1992). The Spring Valley fault offsets alluvial terraces with an NVTD of 5 m, with the most recent earthquakes no younger than ∼17 ka, yielding a maximum late Quaternary rate of 0.25 mm yr^{-1} (Table 1). Assuming 6 km of net vertical slip on the fault since the cessation of motion on the Snake Range detachment as recently as ∼15 Ma, an average slip rate of 0.25 mm yr^{-1} is also obtained (Table 1).

5 GEODETIC AND GEOLOGICAL VELOCITY FIELDS

5.1 Geodetic velocity field

The 1997–2000 horizontal strain field across the eastern Basin and Range is dominantly east–west uniaxial extension (Bennett *et al.* 1999; Wernicke *et al.* 2000; Bennett *et al.* 2003). Within the transect area, the west velocities of CAST, SMEL, FOOT and EGAN increase monotonically westwards to a value of 4.1 mm yr^{-1} relative to a fixed North American reference frame, then remain relatively constant across central Nevada (Fig. 2; Table 3). The increase over the transect is linear with distance. A least-squares regression of west velocity versus longitude through CAST, SMEL, FOOT and EGAN, weighted by errors in individual site velocities, yields a slope of ∼10 nstr yr^{-1}, with scatter of only 0.1 to 0.2 mm yr^{-1} (Fig. 8).

Table 3. BARGEN GPS velocities from western Utah and eastern Nevada.

GPS site	Longitude (°W)	Latitude (°N)	West velocity[a] (mm yr^{-1})	North velocity[a] (mm yr^{-1})
CAST	110.667	39.191	0.26 ± 0.2	0.71 ± 0.2
SMEL	112.845	39.426	2.52 ± 0.3	0.29 ± 0.3
FOOT	113.805	39.369	2.91 ± 0.2	0.43 ± 0.3
EGAN	114.939	39.345	4.13 ± 0.3	0.36 ± 0.4
NEWP	117.509	39.686	4.48 ± 0.3	2.18 ± 0.5
MINE	116.096	40.148	3.99 ± 0.2	0.98 ± 0.4
HEBE	111.373	40.514	0.16 ± 0.2	0.61 ± 0.2
COON	112.121	40.653	1.82 ± 0.2	0.59 ± 0.3
CEDA	112.860	40.681	2.60 ± 0.2	0.32 ± 0.3
GOSH	114.180	40.640	3.02 ± 0.2	0.27 ± 0.3
RUBY	115.123	40.617	2.40 ± 0.2	0.41 ± 0.4
ELKO	115.817	40.915	4.09 ± 0.2	0.59 ± 0.4

[a]Relative to a North America fixed reference frame (e.g. Bennett *et al.* 1999). Errors are 1 std. dev. GPS solution as of 2000 April.

West of EGAN, the two sites nearest latitude 40°N, MINE and NEWP, have west velocities nearly the same as EGAN and define a baseline ∼220 km long, which has negligible strain. Although there may be considerable internal variation across this region, these data suggest that the central part of Nevada is not extending significantly compared with the eastern Basin and Range in east-central Nevada and Utah (Bennett *et al.* 2003).

The GPS baseline from CAST to SMEL, however, encompasses a significant portion of (presumably) stable crust, as site CAST is situated well east of the edge of the Colorado Plateau (Figs 2 and 3). It is therefore possible that the eastern $\frac{1}{3}$ to $\frac{1}{2}$ of the baseline CAST–SMEL has zero strain rate. This inference is supported by BARGEN data farther north, where the site HEBE (Fig. 2), located 30 km east of the Wasatch fault, has nearly the same east velocity with respect to North America as CAST (Bennett *et al.* 1999). If we assume that the velocity of the upper crust is zero between CAST and a point 30 km east of the edge of the Colorado Plateau (analogous to the position of HEBE), then a linear regression can be made between this point and the sites SMEL, FOOT and EGAN. This regression yields a linear strain rate of ∼11 nstr yr^{-1} (Fig. 8). The scatter about this fit is <0.5 mm yr^{-1}, therefore a model with a uniform strain rate of 10 nstr yr^{-1} between CAST and EGAN, with essentially zero strain rate west of EGAN, is consistent with the continuous GPS data in this area, and with regional patterns in both campaign and continuous GPS data from the northern Basin and Range (Thatcher *et al.* 1999; Wernicke *et al.* 2000; Bennett *et al.* 2003).

5.2 Geological velocity field

We use fault dips, fault positions and vertical displacement rates to constrain the velocity field in late Quaternary time. As discussed earlier, it appears that slip rates at the surface provide reasonable estimates for slip rates at depth for relatively planar faults and we therefore derive the horizontal slip rates for faults in the study area by dividing vertical slip rates by the tangent of the fault dip (Fig. 5). Creating a horizontal velocity field for a given fault and fault slip rate requires making an assessment of where, spatially, slip on the fault occurs and how this slip, if it occurs at depth, is mapped upwards through the crust to create a velocity field at the surface of the Earth (Fig. 9). As discussed above, an approach using buried edge dislocations in an elastic half-space (Thatcher *et al.* 1999; Smith *et al.* 2000) is not appropriate for Basin and Range faulting. We therefore consider three alternative methods for deriving a horizontal velocity field at the surface from fault slip rates on buried faults. The first is to plot fault slip rate as a step function, where the velocity field increases by the magnitude of the horizontal fault slip rate at a specified point along the fault plane, which can be anywhere from the surface trace of the fault to the intersection of the fault with the base of the crust (Fig. 9a). A second method would be to linearly distribute slip on the fault over the projection of the fault plane on the surface of the Earth (the distance between the surface trace of the fault and the point on the surface of the Earth vertically above the intersection of the fault plane and the base of the seismogenic crust; Fig. 9b). A third method is to represent the slip as a linear increase in horizontal velocity between the surface projections of its intersection with the base of the seismogenic layer and that of the next structurally higher fault (i.e. slip is distributed over the

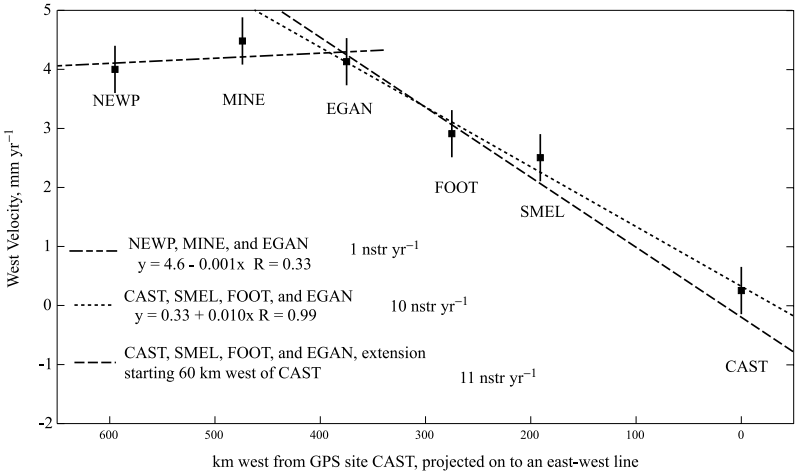

Figure 8. Least-squares regression of the best-fitting line to GPS sites on the eastern end of the BARGEN profile. Three different regressions were calculated. The first two regressions were calculated through the eastern four sites. In one of these regressions, the site CAST was treated as a point in the linear regression. In the other case, we noted that the site HEBE (Fig. 2), which sits considerably closer to the Wasatch fault/Basin and Range breakaway zone than CAST, is not moving west with respect to CAST, suggesting that the Colorado Plateau (Fig. 1) is a stable block. Based on this observation we replaced CAST in our regression with a point that had the same velocity as CAST, but was located 60 km farther west, at the edge of the Basin and Range province. The third regression is from site EGAN to western sites MINE and NEWP. The best-fitting strain rate between EGAN and NEWP is ∼1 nstr yr^{-1}.

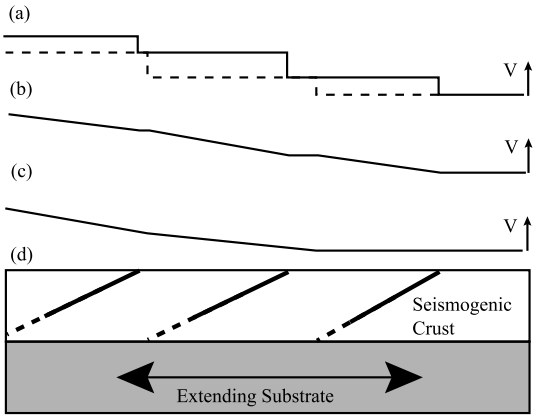

Figure 9. Methods of deriving a velocity field from fault locations and slip rates. (a) The velocity field is created by plotting slip rates as a step function. The solid line is a step function at the intersection of the fault with the surface of the Earth. The dashed line is a step function at the intersection of the fault with the base of the seismogenic crust. (b) The velocity field is created by a linear distribution of slip over the projection of the fault plane on the surface of the Earth. (c) The velocity field is plotted as a linear distribution over the base of each fault block, with slip distributed from the intersection of one fault with the base of the crust to the intersection of the next fault with the base of the crust. (d) Diagram of the position of faults used to make velocity fields (a)–(c).

projection on the surface of the Earth of the bottom of the hanging wall block; Fig. 9c).

The step-function representation would correspond to the case where all deformation is accommodated by fault creep. Because significant fault creep has not been observed in the Basin and Range, it may not be the appropriate method for comparison with geodetic data. The driving mechanism for interseismic strain accumulation, whatever its kinematics, is unlikely to be localized on specific fault planes and thus surface strain is unlikely to be accurately represented by a series of step functions. For comparison with geodetic data, therefore, the second depiction is perhaps more appropriate than the first. If, however, the system behaves roughly as prescribed by Bourne *et al.* (1998), where the motions of geodetic sites correspond directly to the strain applied by the substrate on the base of the seismogenic layer, the third depiction may be most appropriate for comparison to geodetic data, because it reflects the interseismic velocity field closest to its kinematic source. We note that the three methods differ relatively little as regards comparison with sparse geodetic data, and, since it is difficult to advocate one of these three models over the other two, we choose to depict the velocity field as two step functions, one at the surface trace of the fault and another at the intercept of the fault with the base of the crust. Such a depiction envelopes all possible velocity fields produced by any one, or combination, of the three above methods.

Because our data set of vertical slip rates represents maximum slip rates, the horizontal velocity field we derive must also be considered a maximum for seismogenic slip expressed by surface faulting. For several faults, however, the magnitude of the late Holocene slip rate on the fault is substantially greater than the rate estimated for the late Quaternary. In Fig. 10, we show two geological velocity fields for the Sevier Desert transect, one (Fig. 10a) based on maximum vertical slip rates for the Holocene, the other (Fig. 10b) based on maximum vertical slip rates for the late Quaternary. The components of slip on each fault in the transect for both velocity fields are shown in Table 4.

6 DISCUSSION

The principal issues in evaluating these data are, first, whether the extension rate based on geodetic data are consistent with the geological evidence of seismic strain release and, second, whether either data set indicates that strain accumulation is localized across the Intermountain seismic belt (Wasatch and related fault zones), or is more evenly distributed across faults to the west.

6.1 Comparison of geodetic, Holocene and late Quaternary geological velocity fields

We note that of the two geological velocity fields, the late Quaternary maximum velocity field agrees well with the geodetic velocity field, while the Holocene maximum velocity field across the region exceeds the geodetic velocities by more than a factor of 2 (Fig. 10). As discussed above, the maximum rates generally reflect the minimum amount of time over which relatively well constrained displacements occurred. Because the maximum amount of time, and hence minimum slip rates, permit very low velocities, both Holocene and late Quaternary velocity fields are consistent with the geodetic data. However, because the largest component of the Holocene field is based on the 15.2-m offset of an 11-ka basalt flow across the Black Rock fault zone, the minimum rate derived from this particular constraint is not substantially lower than the maximum. The low dip of the Sevier Desert detachment amplifies vertical displacement rates into large horizontal rates according to our assumptions (Fig. 5). However, if the age of the flow and the assumptions of Fig. 5 are not grossly in error ($>$10 per cent), the Holocene slip rate across our transect significantly exceeds the geodetic rate on the basis of this constraint alone.

An additional caveat regarding the Sevier Desert slip rate is that the main strand of the Black Rock fault zone is aligned with a series of Quaternary basaltic cinder cones, suggesting that fault displacement may in some way be related to local magmatic processes rather than motion on the Sevier Desert detachment. Except for their spatial association with the basalts, there is nothing unusual about the slip rates or geometries of these faults relative to other Quaternary faults within or near the Intermountain seismic belt. Although fault scarps are common within some volcanic centres, faults and eruptions are not necessarily cospatial (e.g. fig. 12 of Fridrich 1999). The constructional nature of the basaltic cones and the resistance to erosion of basalt likely results in the preferential preservation of fault scarps in basalt. Therefore, we interpret the Black Rock fault zone as kinematically linked to the Sevier Desert detachment, which at various times in the Quaternary was exploited as a conduit for basaltic magma in the upper levels of the crust.

The discrepancy between the Holocene and late Quaternary velocity fields, although tenuous on the basis of these observations, is in accord with discrepancies between Holocene and late Quaternary rates observed farther north along the Wasatch fault (Machette *et al.* 1992a; Friedrich *et al.* 2003) and the Hebgen Lake fault (Zreda & Noller 1998). The central Wasatch fault zone shows evidence for highly episodic strain release, with recent palaeoseismologic work indicating that vertical displacement rates vary from $\sim$1.6 mm yr^{-1} since $\sim$8 ka to $\sim$0.7 mm yr^{-1} since $\sim$19 ka. Maximum long-term (100s of ka) vertical displacement rates on the central Wasatch fault, however range from 0.2–0.4 mm yr^{-1} (Machette *et al.* 1992a). Similarly, the exposure history of the Hebgen Lake scarp reveals a cluster of earthquakes since $\sim$7 ka, with an average vertical slip rate of 1.0 mm yr^{-1}. Between 7 and 20 ka, there is no recorded displacement, then two events with a total of $\sim$7 m of vertical

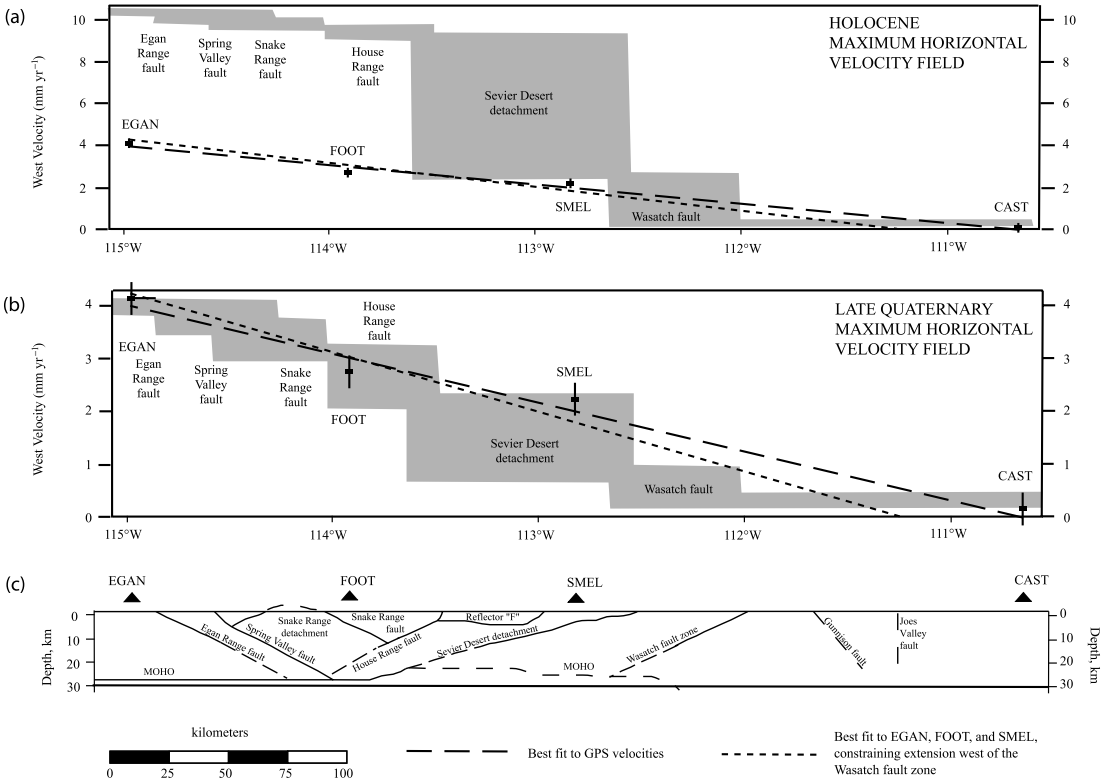

Figure 10. Possible patterns of strain release across the eastern Basin and Range between BARGEN sites CAST and EGAN. Upper bound of grey envelope reflects model where displacement occurs along surface trace, lower bound reflects displacement occurring where the fault intersects the base of the seismogenic layer. Fault slip rates can be found in Table 4. (a) Velocity field for Holocene time. (b) Velocity field for late Quaternary time. (c) Cross-section of actual faults, as observed using seismic reflection data.

Table 4. Components of Quaternary slip on faults between CAST and EGAN.

Fault	Fault Dip	Holocene vertical slip rate (mm yr^{-1})	Holocene horizontal slip rate (mm yr^{-1})	Late Quaternary vertical slip rate (mm yr^{-1})	Late Quaternary horizontal slip rate (mm yr^{-1})
Wasatch	30°	1.3	2.3	0.3	0.5
Sevier Desert[a]	12°	1.4	6.6	0.3	1.4
House Range[b]	30°	0.3	0.4	0.5	0.9
Spring Valley	30°	0.2	0.4	0.3	0.5
Egan Range	30°	0.2	0.4	0.2	0.4

[a]Rates for the Sevier Desert detachment are based on the Devil's Kitchen fault in the Black Rock fault zone. Horizontal slip rates on the Sevier Desert detachment may increase downdip, where the Clear Lake scarps intersect the detachment.
[b]Slip rates for the House Range fault include slip on both the House Range and Drum Mountains scarps.

displacement between ∼20 and 25 ka, preceded by another hiatus of 11 ka with no slip. Hence, the overall vertical slip rate on the Hebgen Lake fault is 0.3 mm yr^{-1}, while the apparent rate during clusters is approximately 1.0 mm yr^{-1} (Zreda & Noller 1998).

The Nephi segment of the Wasatch fault and the Black Rock fault zone each have a maximum vertical slip rate of ∼1.3 mm yr^{-1} over the last 10 ka and a maximum long-term (∼100 ka) slip rate of ∼0.3 mm yr^{-1} (Table 1). Although the constraints on timing of strain release on these two faults are much more sparse than those on the central Wasatch fault, the general pattern appears to be episodic strain release. During such episodes, vertical slip rates may reach as high as ∼1.6 mm yr^{-1}. Between episodes, there may be little or no vertical strain release, such that the long-term average vertical slip rate for the Wasatch fault over several of these episodes is on the order of 0.3 mm yr^{-1} (Friedrich *et al.* 2003).

Issues are (i) whether seismic strain release represents interseismic strain accumulation at the timescale of individual earthquakes (e.g. Reid 1910; Shimazaki & Nakata 1980; Schwartz & Coppersmith 1984) or whether earthquakes are temporally clustered, such that seismic strain release and interseimic strain accumulation only match over many earthquake cycles, or supercycles (Grant & Sieh 1994; Friedrich *et al.* 2003) and (ii) whether we might expect geodetic rates to match either short-term or long-term geological displacement rates.

6.2 Relationship between earthquake clusters and strain accumulation

Does clustering of seismic activity require elastic strain accumulation to fluctuate with time? The total geodetic velocity across the

eastern Basin and Range at the latitude of our transect (3.5–4 mm yr^{-1}) divided by the number of faulted range blocks on a transect from EGAN to CAST (∼ eight range blocks) yields a horizontal slip rate for each range of ∼0.5 mm yr^{-1}. This estimate is in agreement with the rates on the Egan Range, Spring Valley and Wasatch faults, but significantly lower than the rates on the House Range fault and Sevier Desert detachment. However, as described above, the latter two faults encompass a wider portion of the transect than the other faults, carrying one or more additional faults in their hanging walls. Therefore, the plot of maximum late Quaternary rates as a function of distance (Fig. 10) is consistent with a model of uniformly distributed long-term strain accumulation.

If the discrepancy between Holocene and late Quaternary rates is real, then the agreement between the geodetic rate and the late Quaternary rate suggests that the Holocene represents a clustered strain release event, or portion of a supercycle, barring the improbability that a transient period of rapid strain accumulation ended within the last few thousand years. If this were the case, the palaeoseismic evidence for earthquake clustering would then require a model capable of explaining large, short-period fluctuations in strain accumulation rate. It is difficult, however, to envisage a mechanism rooted in variations in large-scale driving forces, such as plate motions or lithospheric buoyancy, that might operate on the 10 000-yr timescale. Rather, strongly variable strain release patterns more likely result from relatively local phenomena related to rheological effects or dynamic fault interactions during steady-state large-scale strain accumulation. Therefore, we interpret strain release rates for relatively long (∼100 ka) timescales as representative of large-scale strain accumulation rates (Friedrich *et al.* 2003).

6.3 Distribution of strain accumulation in the eastern Basin and Range

Our interpretation that strain accumulation is broadly distributed across the ∼350 km width of the eastern Great Basin, from the Wasatch fault to the Egan Range in eastern Nevada (Fig. 10), contrasts with those based on previous geodetic surveys across the Intermountain seismic belt and eastern Great Basin, which have ascribed the majority of the deformation to the Wasatch fault zone (Dixon *et al.* 1995; Martinez *et al.* 1998; Thatcher *et al.* 1999; Dixon *et al.* 2000). The latter interpretation was reasonable on the basis of geodetic data available, but is difficult to reconcile with the continuous GPS data across the region. As demonstrated in a comparison of continuous and campaign GPS data across the Great Basin region, the campaign data overlap the continuous data at the 2σ level, and are consistent with either strongly focused strain near the Wasatch fault or a monotonic increase in velocity between the Colorado Plateau and EGAN (fig. 2c of Wernicke *et al.* 2000). Addressing why strain accumulation in the Basin and Range appears to be broadly distributed within the eastern portion of the province and whether this distribution of strain is similar at other latitudes may be fundamental to understanding the dynamics of extension in the western USA.

BARGEN data from a northern GPS transect (∼40°N) yields a similar strain accumulation distribution to the transect discussed above, but differs in detail (Bennett *et al.* 1999, 2003; Friedrich *et al.* 2003). Sites CEDA and GOSH, which are located at roughly the same longitude as sites SMEL and FOOT, respectively, have similar velocities (Fig. 2; Table 3). However the west velocities of RUBY and EGAN, which also lie at nearly the same longitude, are ∼2.4 and ∼4.1 mm yr^{-1}, respectively, with the baseline GOSH–RUBY showing contraction of ∼0.6 mm yr^{-1} (∼10 nstr yr^{-1}), although within error their velocities may be nearly the same. In addition, the baseline HEBE–COON indicates an extensional strain rate of ∼20–25 nstr yr^{-1}, more than double the average eastern Great Basin rate (Friedrich *et al.* 2003).

Although we cannot absolutely rule out a localization of rapid extensional strain across the southernmost Wasatch fault zone, neither the contractile strain suggested by the baseline GOSH–RUBY in easternmost Nevada, nor the 20–25 nstr yr^{-1} of extensional strain across HEBE–COON is apparent in the southern transect. The reasons for this are uncertain; however, one factor that could potentially affect strain distribution across either of these transects is the occurrence of major seismic events. For example, a large earthquake may have occurred within the last few hundred years on the East Great Salt Lake fault (Dinter & Pechmann, private communication, 2000, Colman *et al.* 2002), which is located at approximately the longitude of site COON (Fig. 2). Such an earthquake can induce transient strain waves in the crust through viscoelastic relaxation effects following the seismic event (e.g. Hager *et al.* 1999; Wernicke *et al.* 2000; Hetland & Hager 2003). The low strain rates in the eastern Great Basin, ∼11 nstr yr^{-1} across the southern transect, with a 25 nstr yr^{-1} maximum near the northern Wasatch fault, would be overwhelmed by strain transients in the recent aftermath of a moderately large earthquake. Indeed, given reasonable physical parameters, viscoelastic effects 200–400 yr after such an event on the East Great Salt Lake fault would result in measurable extension near the rupture, according to a simple 1-D model of an elastic layer on a viscous substrate (for example, fig. 5c in Wernicke *et al.* 2000; Friedrich *et al.* 2003). With the exception of an event on the Nephi segment, which occurred sometime between 500 and 1000 yr ago (Machette *et al.* 1992a), the southern transect has not experienced a significant earthquake for perhaps several millennia (Hecker 1993; McCalpin *et al.* 1996). Thus, the effects of any viscoelastic waves generated by seismic events in this region would be difficult to detect.

Regardless of these details, the geodetic data indicate that strain accumulation from 1997–2000 in the eastern Basin and Range is not limited to the Wasatch fault, or to the Intermountain seismic belt, at 39°N. Rather, it appears that significant strain is distributed across the region west of the Wasatch fault zone.

7 CONCLUSIONS

Both geodetic and geological data appear to define an ∼350-km-wide belt of relatively uniform strain accumulation of ∼10 nstr yr^{-1} east–west extension in the eastern Basin and Range. Velocities of two sites to the west of Ely, Nevada, at this same latitude, appear to define an area across central Nevada with little net internal strain rate, moving at ∼3 mm yr^{-1} relative to the Colorado Plateau. Palaeoseismological data, while sparse over this western region, suggest a large part of it may have been inactive over the last 130 ka or more (Wallace 1984; Dohrenwend *et al.* 1996). The late Quaternary geological velocity field east of EGAN, derived using seismic reflection and neotectonic data, indicate a maximum velocity of Ely with respect to the Colorado Plateau of 4 mm yr^{-1}, evenly distributed across the region. Although the geodetic and late Quaternary geological velocity fields are consistent, the apparent lack of agreement with the relatively rapid Holocene velocity field suggests fault slip clustering may be a standard mechanism of seismic strain release.

Our GPS results are broadly consistent with those of Bennett *et al.* (1998) based on just the first 9 month of continuous GPS data. Considering the combined geodetic and geological velocity fields,

the Intermountain seismic belt does not appear to be the sole locus of extensional strain accumulation within the eastern Great Basin. This result contrasts with earlier suggestions that most or all of the $\sim$3 mm yr^{-1} of displacement between Ely, Nevada and the Colorado Plateau is accommodated along the Wasatch fault zone (Dixon *et al.* 1995; Martinez *et al.* 1998; Thatcher *et al.* 1999; Dixon *et al.* 2000). Our geodetic results limit the horizontal velocity across the southern Wasatch fault to $\sim$2.5 mm yr^{-1}, assuming no slip on the Sevier Desert detachment. However, the geological velocity field suggests a maximum horizontal rate on the Wasatch fault of $\sim$0.5 mm yr^{-1} over the late Quaternary, with most of the remaining deformation accommodated on the Sevier Desert detachment and related faults.

ACKNOWLEDGMENTS

BARGEN research is funded by the National Science Foundation (grants EAR 97-25766, 99-03366 and 00-01209), the Yucca Mountain Project of the US Department of Energy, and the Solid Earth and Hazards Program of NASA. Support for this work was also provided by an NSF Graduate Fellowship (NAN). Network design and maintenance assistance is provided by the University NAVSTAR Consortium (UNAVCO) Facility in Boulder, Colorado, the University of Nevada, Reno, and the University of Utah. We thank Tim Dixon and John Oldow for productive comments on this manuscript.

REFERENCES

Allmendinger, R.W. & Royse, F., Jr, 1995. Is the Sevier Desert reflection of west-central Utah a normal fault?; discussion and reply, *Geology,* **23,** 669–670.

Allmendinger, R.W., Sharp, J.W., Von Tish, D., Serpa, L., Brown, L., Kaufman, S., Oliver, J.E. & Smith, R.B., 1983. Cenozoic and Mesozoic structure of the eastern Basin and Range Province, Utah, from COCORP seismic-reflection data, *Geology,* **11,** 532–536.

Allmendinger, R.W., Farmer, H., Hauser, E.C., Sharp, J., von Tish, D., Oliver, J. & Kaufman, S., 1986. Phanerozoic tectonics of the Basin and Range-Colorado Plateau transition from COCORP data and geological data; a review, in *Reflection seismology; the continental crust*, Geodynamics Series, Vol. 14, pp. 257–267, eds Barazangi, M. & Brown, L.D., American Geophysical Union, Washington, DC.

Allmendinger, R.W., Hauge, T.A., Hauser, E.C., Potter, C.J., Klemperer, S.L., Nelson, K.D., Knuepfer, P.L.K. & Oliver, J., 1987. Overview of the COCORP 40°N transect, western United States: the fabric of an orogenic belt, *Bull. geol. Soc. Am.,* **98,** 308–319.

Anders, M.H. & Christie-Blick, N., 1994. Is the Sevier Desert reflection of west-central Utah a normal fault?, *Geology,* **22,** 771–774.

Anderson, R.E., 1983. *Cenozoic structural history of selected areas in the eastern Great Basin, Nevada-Utah*, Open file report 83-0504, US Geological Survey, Denver, CO.

Barrientos, S.E., Stein, R.S. & Ward, S.N., 1987. Comparison of the 1959 Hebgen Lake, Montana, and the 1983 Borah Peak, Idaho, earthquakes from geodetic observations, *Bull. seism. Soc. Am.,* **77,** 784–808.

Bartley, J.M. & Wernicke, B.P., 1984. The Snake Range decollement interpreted as a major extensional shear zone, *Tectonics,* **3,** 647–657.

Bennett, R.A., Rodi, W. & Reilinger, R.E., 1996. Global Positioning System constraints on fault slip rates in Southern California and northern Baja, Mexico, *J. geophys. Res.,* **101,** 21 943–21 960.

Bennett, R.A., Wernicke, B.P. & Davis, J.L., 1998a. Continuous GPS measurements of contemporary deformation across the northern Basin and Range, *Geophys. Res. Lett.,* **25,** 563–566.

Bennett, R.A., Davis, J.L. & Wernicke, B.P., 1999. Present-day pattern of Cordilleran deformation in the Western United States, *Geology,* **27,** 371–374.

Bennett, R.A., Davis, J.L., Wernicke, B.P. & Normandeau, J.E., 2002. Space geodetic measurements of plate boundary deformation in the western U.S. Cordillera, in *Plate Boundary Zones*, Geodynamics Series, Vol. 30, pp. 27–55, eds Stein, S.A. & Freymueller, J.T., American Geophysical Union, Washington, DC.

Bennett, R.A., Wernicke, B.P., Niemi, N.A., Friedrich, A.M. & Davis, J.L., 2003. BARGEN continuous GPS data, *Tectonics,* **22,** 1008, doi:10.1029/2001TC001355.

Bourne, S.J., England, P.C. & Parsons, B., 1998. The motion of crustal blocks driven by flow of the lower lithosphere and implications for slip rates of continental strike-slip faults., *Nature,* **391,** 655–659.

Bruhn, R.L. & Schultz, R.A., 1996. Geometry and slip distribution in normal fault systems; implications for mechanics and fault-related hazards, *J. geophys. Res.,* **101,** 3401–3412.

Bruhn, R.L., Gibler, P.R., Houghton, W. & Parry, W.T., 1992. Structure of the Salt Lake segment, Wasatch normal fault zone: Implications for rupture propagation during normal faulting, in *Assessment of regional earthquake hazards and risk along the Wasatch Front, Utah,* Professional Paper 1500-H, pp. H1–H25, eds Gori, P.L. & Hays, W.W., US Geological Survey, Reston, VA.

Bucknam, R.C. & Anderson, R.E., 1979a. Estimation of fault-scarp ages from a scarp-height-slope-angle relationship, *Geology,* **7,** 11–14.

Bucknam, R.C. & Anderson, R.E., 1979b. *Map of fault scarps on unconsolidated sediments, Delta 1° by 2° quadrangle, Utah*, scale 1:250 000, Open file report 79-366, US Geological Survey, Denver, CO.

Burchfiel, B.C., Lipman, P.W. & Zoback, M.L., eds., 1992. *The Cordilleran Orogen; conterminous U.S., The geology of North America,* Vol. G-3, Geological Society of America, Boulder, CO.

Caskey, S.J., 1996. Surface faulting, static stress changes, and earthquake triggering during the 1954 Fairview Peak ($M_s = 7.2$) and Dixie Valley ($M_s = 6.8$) earthquakes, central Nevada, *PhD thesis,* University of Nevada, Reno.

Chang, W.L., 1998. Earthquake hazards on the Wasatch fault: tectonically induced flooding and stress triggering of earthquakes, *MS thesis,* University of Utah, Salt Lake City.

Coleman, D.S. & Walker, J.D., 1994. Modes of tilting during extensional core complex development, *Science,* **263,** 215–218.

Coleman, D.S., Bartley, J.M., Walker, J.D., Price, D.E. & Friedrich, A.M., 1997. Extensional faulting, footwall deformation and plutonism in the Mineral Mountains, Southern Sevier Desert, *Brigham Young Univ. geol. Stud.,* **42,** 203–233.

Colman, S.M., Kelts, K.R. & Dinter, D.A., 2002. Depositional history and neotectonics in Great Salt Lake, Utah, from high-resolution seismic stratigraphy, *Sed. Geol.,* **148,** 61–78.

Condie, K.C. & Barsky, C.K., 1972. Origin of Quaternary basalt from the Black Rock desert region, Utah, *Bull. geol. Soc. Am.,* **83,** 333–352.

Coogan, J.C. & DeCelles, P.G., 1996. Extensional collapse along the Sevier Desert reflection, northern Sevier Desert basin, Western United States, *Geology,* **24,** 933–936.

Crone, A.J., 1983. Amount of displacement and estimated age of a Holocene surface faulting event, eastern Great Basin, Millard County, Utah, in *Geologic excursions in neotectonics and engineering geology in Utah; Guidebook, Part IV*, Spec. Stud. Utah geol. miner. Surv., Vol. 62, pp. 49–55, ed. Gurgel, K.D., Utah Geological Survey, Salt Lake City, UT.

Crone, A.J. & Harding, S.T., 1984. Relationship of late Quaternary fault scarps to subjacent faults, eastern Great Basin, Utah, *Geology,* **12,** 292–295.

Crone, A.J., Machette, M.N., Bonilla, M.G., Lienkaemper, J.J., Pierce, K.L., Scott, W.E. & Bucknam, R.C., 1987. Surface faulting accompanying the Borah Peak earthquake and segmentation of the Lost River Fault, central Idaho, *Bull. seism. Soc. Am.,* **77,** 739–770.

Currey, D.R., 1982. *Lake Bonneville; selected features of relevance to neotectonic analysis*, Open file report 82-1070, US Geological Survey, Dever, CO.

Davis, J.L., Bennett, R.A. & Wernicke, B.P., 2003. Assessment of GPS velocity accuracy for the Basin and Range Geodetic Network (BARGEN), *Geophys. Res. Lett.,* **30,** 10.1029/2003GL016961.

Dinter, D.A. & Pechmann, J.C., 2000. Late Quaternary slip rates and recurrence intervals of large earthquakes on the East Great Salt Lake normal fault, Utah: Estimates from high resolution seismic reflection data, *Abs. prog. geol. Soc. Am.,* **32,** 7, A507.

Dixon, T.H., Robaudo, S., Lee, J. & Reheis, M.C., 1995. Constraints on present-day Basin and Range deformation from space geodesy, *Tectonics,* **14,** 755–772.

Dixon, T.H., Miller, M., Farina, F., Wang, H. & Johnson, D., 2000. Present-day motion of the Sierra Nevada block and some tectonic implications for the Basin and Range province, North American Cordillera, *Tectonics,* **19,** 1–24.

Dohrenwend, J.C., Schell, B.A. & Moring, B.C., 1992. *Reconnaissance photogeologic map of young faults in the Ely 1° by 2° quadrangle, Nevada and Utah,* scale 1:250 000, Misc. Field Stud. Map MF-2181, US Geological Survey, Washington, DC.

Dohrenwend, J.C., Schell, B.A., Menges, C.M., Moring, B.C. & McKittrick, M.A., 1996. Reconnaissance photogeologic map of young (Quaternary and late Tertiary) faults in Nevada, in *An analysis of Nevada's metal-bearing mineral resources,* Open file report, Vol. 96-2, pp. 9.1–9.12, ed. Singer, D.A., Nevada Bureau of Mines and Geology, Reno, NV.

England, P. & McKenzie, D., 1982. A thin viscous sheet model for continental deformation, *Geophys. J. R. astr. Soc.,* **70,** 295–321.

Ertec Western, Inc., 1981. *Faults and lineaments in the MX siting region, Nevada and Utah,* Vols 1 and 2, Ertec Western, Inc., Long Beach, CA.

Eyidogan, H. & Jackson, J., 1985. A seismological study of normal faulting in the Demirci, Alasehir and Gediz earthquakes of 1969–70 in western Turkey; implications for the nature and geometry of deformation in the continental crust, *Geophys. J. R. astr. Soc.,* **81,** 569–607.

Fong, A.W., 1991. Fountain Green South Quadrangle, Juab and San Pete Counties, Utah, in *Utah Geological and Mineral Survey Open file report 204*, scale 1:24 000, Utah Geological and Mineral Survey, Salt Lake City, UT.

Fridrich, C.J., 1999. Tectonic evolution of Crater Flat basin, Yucca Mountain, Nevada, in *Cenozoic basins of the Death Valley region,* Vol. 333, pp. 169–195, eds Wright, L.A. & Troxel, B.W., Geological Society of America, Boulder, CO.

Friedrich, A.M., Wernicke, B.P., Niemi, N.A., Bennett, R.A. & Davis, J.L., 2003. Comparison of geodetic and geologic data from the Wasatch region, Utah, and implications for the spectral character of Earth deformation at periods of ten to ten million years, *J. geophys. Res.,* **108,** 2199, doi:10.1029/2001JB000682.

Gans, P.B., Miller, E.L., McCarthy, J. & Ouldcott, M.L., 1985. Tertiary extensional faulting and evolving ductile-brittle transition zones in the northern Snake Range and vicinity; new insights from seismic data, *Geology,* **13,** 189–193.

Grant, L.B. & Sieh, K., 1994. Paleoseismic evidence of clustered earthquakes on the San Andreas fault in the Carrizo Plain, California, *J. geophys. Res.,* **99,** 6819–6841.

Hager, B.H., Lyzenga, G.A., Donnellan, A. & Dong, D., 1999. Reconciling rapid strain accumulation with deep seismogenic fault planes in the Ventura Basin, California, *J. geophys. Res.,* **104,** 25 207–25 219.

Hauser, E. *et al.*, 1987. Crustal structure of eastern Nevada from COCORP deep seismic reflection data, *Bull. geol. Soc. Am.,* **99,** 833–844.

Hecker, S., 1993. Quaternary tectonics of Utah with emphasis on earthquake-hazard characterization, *Bull. Utah geol. Surv.,* **127**, 157 pp.

Herring, T.A., 1999. *GLOBK: Global Kalman filter VLBI and GPS analysis program*, Massachusetts Institute of Technology, Cambridge, MA.

Hetland, E.A. & Hager, B.H., 2003. Postseismic relaxation across the Central Nevada Seismic Belt, *J. geophys. Res.,* **108,** 2394, doi:10.1029/2002JB002257.

Hintze, L.F., 1988. *Geologic history of Utah*, Brigham Young University, Provo, UT.

Hodgkinson, K.M., Stein, R.S. & King, G.C.P., 1996. The 1954 Rainbow Mountain-Fairview Peak-Dixie Valley earthquakes; a triggered normal faulting sequence, *J. geophys. Res.,* **101,** 25 459–25 471.

Hoover, J.D., 1974. Periodic Quaternary volcanism in the Black Rock Desert, Utah, *Brigham Young Univ. geol. Stud.,* **21,** 3–72.

Hubert, A., King, G., Armijo, R., Meyer, B. & Papanastasiou, D., 1996. Fault re-activation, stress interaction and rupture propagation of the 1981 Corinth earthquake sequence, *Earth planet. Sci. Lett.,* **142,** 573–585.

Jackson, J.A., 1987. Active normal faulting and crustal extension, in *Continental extensional tectonics,* Vol. 28, pp. 3–17, eds Coward, M.P., Dewey, J.F. & Hancock, P.L., Geological Society of London, London, UK.

Jackson, J.A., Gagnepain, J., Houseman, G., King, G.C.P., Papadimitriou, P., Soufleris C. & Virieux, J., 1982. Seismicity, normal faulting, and the geomorphological development of the Gulf of Corinth (Greece); the Corinth earthquakes of February and March 1981, *Earth planet. Sci. Lett.,* **57,** 377–397.

Jackson, M., 1991. The number and timing of Holocene paleoseismic events on the Nephi and Levan segments, Wasatch fault zone, Utah, in *Paleoseismology of Utah,* Vol. 3, Utah Geological and Mineral Survey, Salt Lake City, UT.

King, R.W. & Bock, Y., 1999. *Documentation for the MIT GPS analysis software: GAMIT*, Massachusetts Institute of Technology, Cambridge, MA.

Langbein, J. & Johnson, H., 1995. Noise level of geodetic monuments, *EOS, Trans. Am. geophys. Un.,* **76,** 142.

Langbein, J.L., Wyatt, F., Johnson, H., Hamann, D. & Zimmer, P., 1995. Improved stability of a deeply anchored geodetic monument for deformation monitoring, *Geophys. Res. Lett.,* **22,** 3533–3536.

Larson, K.M., Freymueller, J.T. & Philipsen, S., 1997. Global plate velocities from the Global Positioning System, *J. geophys. Res.,* **102,** 9961–9981.

Lee, J., 1995. Rapid uplift and rotation of mylonitic rocks from beneath a detachment fault; insights from potassium feldspar $^{40}Ar/^{39}Ar$ thermochronology, northern Snake Range, Nevada, *Tectonics,* **14,** 54–77.

Lewis, C.J., Wernicke, B.P., Selverstone, J. & Bartley, J.M., 1999. Deep burial of the footwall of the northern Snake Range decollement, Nevada, *Bull. geol. Soc. Am.,* **111,** 39–51.

Lowry, A.R. & Smith, R.B., 1995. Strength and rheology of the western U.S. Cordillera, , *J. geophys. Res.,* **100,** 17 947–17 963.

Ma, C., Ryan, J.W., Gordon, D., Caprette, D.S. & Himwich, W.E., 1993. Reference frames from CDP VLBI data, in *Contributions of space geodesy to geodynamics; Earth dynamics,* Vol. 24, pp. 121–145, eds Smith, D.E. & Turcotte, D.L., American Geophysical Union, Washington, DC.

McCalpin, J.P. & Nishenko, S.P., 1996. Holocene paleoseismicity, temporal clustering, and probabilities of future large ($M > 7$) earthquakes on the Wasatch fault zone, Utah, *J. geophys. Res.,* **101,** 6233–6253.

McDonald, R.E., 1976. Tertiary tectonics and sedimentary rocks along the transition: Basin and Range province to plateau and thrust belt province, Utah, in *Geology of the Cordilleran Hingeline*, pp. 281–317, ed. Hill, J.G., Rocky Mountain Association of Geologists, Denver, CO.

Machette, M.N., Personius, S.F., Nelson, A.R., Schwartz, D.P. & Lund, W.R., 1991. The Wasatch fault zone, Utah; segmentation and history of Holocene earthquakes, *J. struct. Geol.,* **13,** 137–149.

Machette, M.N., Personius, S.F. & Nelson, A.R., 1992a. Paleoseismology of the Wasatch fault zone; a summary of recent investigations, interpretations, and conclusions, in *Assessment of regional earthquake hazards and risk along the Wasatch Front, Utah,* Professional Paper 1500-A, pp. A1–A71, eds Gori, P.L. & Hays, W.W., US Geological Survey, Reston, VA.

Machette, M.N., Personius, S.F., Nelson, A.R., Bucknam, R.C. & Hancock, P.L., 1992b. The Wasatch fault zone, U.S.A., *Annales Tectonicae,* **6,** Suppl., 5–39.

Martinez, L.J., Meertens, C.M. & Smith, R.B., 1998. Rapid deformation rates along the Wasatch fault zone, Utah, from first GPS measurements with implications for earthquake hazard, *Geophys. Res. Lett.,* **25,** 567–570.

Matsu'ura, M., Jackson, D.D. & Cheng, A., 1986. Dislocation model for aseismic deformation at Hollister, California, *J. geophys. Res.,* **91,** 12 661–12 674.

Mattson, A. & Bruhn, R.L., 2001. Fault slip-rates and initiation age based on diffusion equation modeling: Wasatch fault zone and eastern Great Basin, *J. geophys. Res.,* **106,** 13 739–13 750.

Miller, E.L., Dumitru, T.A., Brown, R.W. & Gans, P.B., 1999. Rapid Miocene slip on the Snake Range-Deep Creek Range fault system, east-central Nevada, *Bull. geol. Soc. Am.,* **111,** 886–905.

Misch, P., 1960. Regional structural reconnaissance in central-northeast Nevada and some adjacent areas–Observations and interpretations, in *Guidebook to the geology of east central Nevada*, pp. 17–42, eds Boettcher, J.W. & Sloan, W.W., Jr., Intermountain Association of Petroleum Geologists, Salt Lake City, UT.

Myers, W.B. & Hamilton, W., 1964. Deformation accompanying the Hebgen Lake earthquake of August 17, 1959, in *The Hebgen Lake, Montana, earthquake of August 17, 1959*, Professional paper 435-I, pp. 55–98, US Geological Survey, Washington, DC.

Okada, Y., 1985. Surface deformation due to shear and tensile faults in a half-space, *Bull. seism. Soc. Am.,* **75,** 1135–1154.

Otton, J.K., 1995. Western frontal fault of the Canyon Range; is it the breakaway zone of the Sevier Desert detachment?, *Geology,* **23,** 547–550.

Oviatt, C.G., 1989. *Quaternary geology of part of the Sevier Desert, Millard County, Utah*, Spec. Stud. 70, Utah Geological and Mineral Survey, Salt Lake City, UT.

Oviatt, C.G., 1991. *Quaternary geology of the Black Rock desert, Millard County, Utah*, Spec. Stud. 73, Utah Geological and Mineral Survey, Salt Lake City, UT.

Oviatt, C.G., 1992. *Quaternary geology of the Scipio Valley area, Millard and Juab Counties, Utah*, Spec. Stud. 79, Utah Geological and Mineral Survey, Salt Lake City, UT.

Piekarski, L., 1980. Relative age determination of Quaternary fault scarps along the southern Wasatch, Fish Springs, and House ranges, Utah, *Brigham Young Univ. geol. Stud.,* **27,** 123–139.

Planke, S. & Smith, R.B., 1991. Cenozoic extension and evolution of the Sevier Desert basin, Utah, from seismic reflection, gravity, and well log data, *Tectonics,* **10,** 345–365.

dePolo, C.M., 1998. A reconnaissance technique for estimating the slip rates of normal-slip faults in the Great Basin, and application to faults in Nevada, USA, *PhD thesis,* University of Nevada, Reno.

Reid, H.R., 1910. The mechanics of the earthquake, in *The California earthquake of April 18, 1906, Report of the State Earthquake Investigation Commission,* Vol. 2, pp. 1–192, Carnegie Institution, Washington, DC.

Rosendahl, B.R., 1987. Architecture of continental rifts with special reference to East Africa, *A. Rev. Earth planet. Sci.,* **15,** 445–503.

Sack, D., 1990. Quaternary geology of Tule Valley, west-central Utah, *Map Utah geol. miner. Surv.,* **124,** scale 1:100,000.

Savage, J.C., 1980. Dislocations in seismology, in *Moving dislocations*, pp. 251–339, ed. Nabarro, F.R.N., *Dislocations in Solids,* **3,** North-Holland Publ. Co., Amsterdam, Netherlands.

Savage, J.C., 1983. Strain accumulation in Western United States, *Ann. Rev. Earth planet. Sci.,* **11,** 11–43.

Savage, J.C. & Hastie, L.M., 1966. Surface deformation associated with dip-slip faulting, *J. geophys. Res.,* **71,** 4897–4904.

Savage, J.C. & Prescott, W.H., 1978. Asthenosphere readjustment and the earthquake cycle, *J. geophys. Res.,* **83,** 3369–3376.

Savage, J.C., Lisowski, M. & Prescott, W.H., 1992. Strain accumulation across the Wasatch Fault near Ogden, Utah, *J. geophys. Res.,* **97,** 2071–2083.

Savage, J.C., Lisowski, M. & Prescott, W.H., 1996. Observed discrepancy between Geodolite and GPS distance measurements, *J. geophys. Res.,* **101,** 25 547–25 552.

Schneider, C.L., Hummon, C., Yeats, R.S. & Huftile, G.J., 1996. Structural evolution of the northern Los Angeles Basin, California, based on growth strata, *Tectonics,* **15,** 341–355.

Scholz, C.H., 1990. *The Mechanics of Earthquakes and Faulting*, Cambridge University Press, Cambridge.

Schwartz, D.P. & Coppersmith, K.J., 1984. Fault behavior and characteristic earthquakes; examples from the Wasatch and San Andreas fault zones, *J. geophys. Res.,* **89,** 5681–5698.

Schwartz, D.P., Hanson, K.L. & Swan, F.H., 1983. Paleoseismic investigations along the Wasatch fault zone: an update, in *Geologic excursions in neotectonics and engineering geology in Utah; Guidebook, Part IV*, Spec. Stud. Utah geol. miner. Surv., Vol. 62, pp. 45–47, ed.Gurgel, K.D., Utah Geological Survey, Salt Lake City, UT.

Sharp, J.W., 1984. West-central Utah; palinspastically restored sections constrained by Cocorp seismic reflection data, *MS thesis,* Cornell University, Ithaca, NY.

Shimazaki, K. & Nakata, T., 1980. Time-predictable recurrence model for large earthquakes, *Geophys. Res. Lett.,* **7,** 279–282.

Smith, R.B. & Bruhn, R.L., 1984. Intraplate extensional tectonics of the eastern Basin-Range; inferences on structural style from seismic reflection data, regional tectonics, and thermal-mechanical models of brittle-ductile deformation, *J. geophys. Res.,* **89,** 5733–5762.

Smith, R.B. & Sbar, M.L., 1974. Contemporary tectonics and seismicity of the western United States with emphasis on the Intermountain seismic belt, *Bull. geol. Soc. Am.,* **85,** 1205–1218.

Smith, R.B., Chang, W.L. & Meertens, C.M., 2000. Neotectonics of the Wasatch fault from rheology, paleoseismicity, and GPS measurements, *Abs. geol. Soc. Am.,* **32,** 7, A507.

Standlee, L.A., 1982. Structure and stratigraphy of Jurassic rocks in central Utah: their influence on tectonic development of the Cordilleran foreland and thrust belt, in *Geologic studies of the Cordilleran thrust belt,* Vol. 1, pp. 357–382, ed. Powers, R.B., Rocky Mountain Association of Geologists, Denver, CO.

Stewart, J.H., 1978. Basin–range structure in western North America; a review, *Mem. geol. Soc. Am.,* **152,** 1–31.

Stockli, D.F., 1999. Regional timing and spatial distribution of Miocene extension in the northern Basin and Range province, *PhD thesis,* Stanford University, Palo Alto, CA.

Stockli, D.F., Linn, J.K., Walker, J.D. & Dumitru, T.A., 2001. Miocene unroofing of the Canyon Range during extension along the Sevier Desert detachment, west-central Utah, *Tectonics,* **20,** 289–307.

Thatcher, W., 1983. Nonlinear strain buildup and the earthquake cycle on the San Andreas Fault, *J. geophys. Res.,* **88,** 5893–5902.

Thatcher, W., 1990. Present-day crustal movements and the mechanics of cyclic deformation, in *The San Andreas fault system, California,* Professional paper 1515, pp. 189–205, ed. Wallace, R.E., US Geological Survey, Reston, VA.

Thatcher, W., 1995. Microplate versus continuum descriptions of active tectonic deformation, *J. geophys. Res.,* **100,** 3885–3894.

Thatcher, W. & Bonilla, M.G., 1989. *Earthquake fault slip estimation from geologic, geodetic, and seismologic observations; implications for earthquake mechanics and fault segmentation*, Open file report 89-315, US Geological Survey, Denver, CO.

Thatcher, W., Foulger, G.R., Julian, B.R., Svarc, J., Quilty, E. & Bawden, G.W., 1999. Present-day deformation across the Basin and Range Province, Western United States, *Science,* **283,** 1714–1718.

Turley, C.H. & Nash, W.P., 1980. *Petrology of Late Tertiary and Quaternary volcanism in western Juab and Millard Counties, Utah*, Spec. Stud. 52, Utah Geological and Mineral Survey, Salt Lake City, UT.

Verrall, P., 1981. *Structural interpretation with application to North Sea problems*, Course notes 3, Joint Association for Petroleum Exploration Courses, London, UK.

Von Tish, D.B., Allmendinger, R.W. & Sharp, J.W., 1985. History of Cenozoic extension in central Sevier Desert, west-central Utah, from COCORP seismic reflection data, *Am. Assoc. Petrol. Geol. Bull.,* **69,** 1077–1087.

Wallace, R.E., 1984. Patterns and timing of late Quaternary faulting in the Great Basin Province and relation to some regional tectonic features, *J. geophys. Res.,* **89,** 5763–5769.

Wallace, R.E., 1987. Grouping and migration of surface faulting and variations in slip rates on faults in the Great Basin Province, *Bull. seism. Soc. Am.,* **77,** 868–876.

Ward, S.N., 1998. On the consistency of earthquake moment rates, geological fault data, and space geodetic strain: the United States, *Geophys. J. Int.,* **134,** 172–186.

Wernicke, B., 1981. Low-angle normal faults in the Basin and Range Province; nappe tectonics in an extending orogen, *Nature,* **291,** 645–648.

Wernicke, B., 1995. Low-angle normal faults and seismicity; a review, *J. geophys. Res.,* **100,** 20 159–20 174.

Wernicke, B. & Burchfiel, B.C., 1982. Modes of extensional tectonics, *J. struct. Geol.,* **4,** 105–115.

Wernicke, B.P., Bennett, R.A., Davis, J.L., Niemi, N.A., House M.A., Abolins, M.I. & Brady, R.J., 1998. Building Large-Scale Continuous GPS Networks, *EOS, Trans. Am. geophys. Un.,* **79,** F206.

Wernicke, B.P., Friedrich, A.M., Niemi, N.A., Bennett, R.A. & Davis, J.L., 1999. Apparent range-normal shortening across the north-central Basin and Range from BARGEN continuous GPS data, *EOS, Trans. Am. geophys. Un.,* **80,** F269.

Wernicke, B.P., Friedrich, A.M., Niemi, N.A., Bennett, R.A. & Davis, J.L., 2000. Dynamics of plate boundary fault systems from Basin and Range Geodetic Network (BARGEN) and geologic data, *GSA Today,* **10,** 11, 1–7.

White, N.J., Jackson, J.A. & McKenzie, D.P., 1986. The relationship between the geometry of normal faults and that of the sedimentary layers in their hanging walls, *J. struct. Geol.,* **8,** 897–909.

Witkind, I.J., 1964. Reactivated faults north of Hebgen Lake, in *The Hebgen Lake, Montana, earthquake of August 17, 1959*, Prof. pap. 435, pp. 37–50, US Geological Survey, Washington, DC.

Witkind, I.J. & Weiss, M.P., 1991. *Geologic map of the Nephi* 30′ × 60′ *Quadrangle, Carbon, Emery, Juab, Sanpete, Utah, and Wasatch counties, Utah*, scale 1:100 000, Misc. Invest. Map I-1631, US Geological Survery, Washington, DC.

Witkind, I.J., Weiss, M.P. & Brown, T.L., 1987. *Geologic map of the Manti* 30′ × 60′ *quadrangle, Carbon, Emery, Juab, Sanpete, and Sevier Counties, Utah*, scale 1:100 000, Misc. Invest. Map I-1631, US Geological Survery, Washington, DC.

Wyatt, F., 1982. Displacement of surface monuments; horizontal motion., *J. geophys. Res.,* **87,** 979–989.

Zreda, M. & Noller, J.S., 1998. Ages of prehistoric earthquakes revealed by cosmogenic chlorine-36 in a bedrock fault scarp at Hebgen Lake, *Science,* **282,** 1097–1099.

APPENDIX A: PALAEOSEISMIC DATA

Vertical fault slip rates have been estimated based on published original data and slip-rate compilations (e.g. Dohrenwend *et al.* 1992; Machette *et al.* 1992a; Hecker 1993; McCalpin & Nishenko 1996; Chang 1998). We determined maximum slip rates, where possible, for order of magnitude time bins from ∼1 Ma to the present (Table 1). At localities where only one offset datum is known, the slip rate was calculated as the long-term average between the age of the offset datum and present day. In these cases, slip distribution through time is not recoverable, allowing the possibility that for a short time fault slip rates were much higher or lower than estimated here. Where two or more offset markers have been dated at a single locality, we have calculated the maximum viable slip rate based on the best linear fit through the data. Fault-slip rates calculated in this way are generally more robust and are shown in bold face type (Table 1).

A1 Wasatch fault—Nephi segment

Three Holocene surface ruptures have been recorded in alluvial deposits exposed in trenches along the Nephi segment of the Wasatch fault (Schwartz *et al.* 1983; Schwartz & Coppersmith 1984; Jackson 1991; Machette *et al.* 1992a). The three rupture events identified along this segment occurred at 1.15 ± 0.07, 3.86 ± 0.24 and $>4.75 \pm 0.20$ ka, with net vertical tectonic displacements (NVTDs) of 2.1 ± 0.1, 2.1 ± 0.1 and 2.6 ± 0.2 m, respectively (McCalpin & Nishenko 1996; Chang 1998). On the 10^2-yr timescale, the maximum slip rate is 1.9 mm yr^{-1}, based on the time elapsed between the most recent event (MRE) and the present day. A more representative Holocene (10^3-yr timescale) slip rate of 1.34 mm yr^{-1} was calculated based on the average rate for the last three events without extrapolating to the present day. An average maximum slip rate for the Nephi segment was calculated by Mattson & Bruhn (2001) based on nonlinear diffusion modelling of composite fault scarps. The modelling results yielded a variation in slip rate from 0.6 mm yr^{-1} between ∼35 and 4.5 ka, and ∼0.3 mm yr^{-1} between 70 and 35 ka. The long-term (10^5 yr) slip rate on the Nephi segment was estimated by Machette *et al.* (1992a) based on a 30-m offset in 150 to 200 ka alluvial fans as ∼0.2 mm yr^{-1}.

A2 Wasatch fault—Levan segment

The Holocene faulting record of the Levan segment is most complete at the Skinners Peak trench site (Schwartz & Coppersmith 1984; Jackson 1991; Machette *et al.* 1992a). The MRE was dated at ∼1 ka by Jackson (1991) and a minimum age for the penultimate event (PUE) is 7.3 ka, based on correlation of events with those recorded at the Deep Creek trench site (Schwartz & Coppersmith 1984). The NVTD for both events is approximately 2 m (Schwartz & Coppersmith 1984; Jackson 1991). The maximum viable slip rate since the MRE (10^2-yr timescale) is 2 mm yr^{-1}. For the mid-Holocene (10^3-yr timescale) the maximum vertical slip rate is 0.35 mm yr^{-1}, based on the difference in time and displacement between the MRE and the PUE.

A3 Wasatch fault—Fayette segment

The Fayette segment probably has not ruptured in at least 10 ka. The MRE may have occurred ∼10 to 15 ka ago, determined empirically by Machette *et al.* (1992a), using the method of Bucknam & Anderson (1979a). Assuming an NVTD of ∼2 m and that only one event occurred in the earliest Holocene or latest Pleistocene, the maximum vertical slip rate is 0.2 mm yr^{-1}.

A4 Gunnison fault

The Gunnison fault experienced late Holocene motion, based on alluvial-surface morphology, its geomorphic position and ^{14}C dating (Witkind *et al*. 1987; Fong 1991; Witkind & Weiss 1991; see also references in Hecker 1993). The MRE, with an NVTD of less than 1 m, may have occurred ∼370 yr ago, based on a ^{14}C date of wood from a tufa deposit.

A5 Pavant Range faults

East-dipping fresh scarps along the eastern side of the Pavant Range may be of Holocene age (Oviatt 1992; Hecker 1993).

A6 Sevier Desert detachment—Canyon Range

During Miocene time, extensional faulting along the Sevier Desert detachment resulted in unroofing of the Canyon Range. Apatite fission-track cooling ages sampled across the range are ∼19 to 15 Ma (Stockli *et al.* 2001). Assuming a geothermal gradient of 20 to 30 °C km^{-1}, approximately 3.5 to 7 km of unroofing of the Canyon Range has occurred since the early Miocene. If denudation directly reflects movement along the Sevier Desert detachment, the maximum vertical fault slip rates are 0.5 and 0.35 mm yr^{-1} for the time interval between 19 to 15 Ma and 19 Ma to the present day, respectively (Stockli *et al.* 2001).

Von Tish *et al.* (1985) calculated a horizontal slip rate across the Sevier Desert detachment of 0.4 to 1.9 mm yr^{-1}, based on the palinspastic cross-section of Sharp (1984) and the seismically observed offset across a 4-Ma basalt flow. Assuming that the Sevier Desert detachment dips ∼15°, the vertical slip rate on the detachment is between 0.1 and 0.5 mm yr^{-1}. However, the lack of late

Pleistocene and Holocene faulting near the surface projection of the Sevier Desert detachment has been explained by west-stepping of the active fault trace into the Sevier Desert Basin with current faulting along, for example, the Black Rock fault zone (Hoover 1974) and the Clear Lake scarps (Von Tish *et al.* 1985).

A7 Clear Lake scarps (Sevier Desert)

The Clear Lake scarps cut pre-Bonneville, Bonneville and early Holocene deposits, and range in surface offset between 2 and 3 m (Currey 1982; Crone & Harding 1984; Oviatt 1989; Hecker 1993). Assuming that the 3-m scarp formed since ∼12 ka, the maximum vertical slip rate is 0.25 mm yr^{-1}. Based on seismic reflection data, a 4-Ma basalt flow is offset ∼760 m, yielding a maximum vertical slip component across the Clear Lake scarps of 0.2 mm yr^{-1} over the last 4 Ma (Crone & Harding 1984; Von Tish *et al.* 1985).

A8 Black Rock fault zone

The Black Rock fault zone cuts lava flows dated from the early Pleistocene to the late Holocene and is inferred to cut lacustrine deposits, also of late Holocene age (Condie & Barsky 1972; Hoover 1974; Oviatt 1989, 1991; Hecker 1993). The largest (67 m) scarps are developed in lava flows of the Beaver Ridge field, which have been dated at 918 ka, yielding an average slip rate of 0.1 mm yr^{-1} through most of the Quaternary. Lava flows of the Pavant field (128 ka) have been offset 18.3 m, but Bonneville shorelines (∼17 ka) have not been disturbed, suggesting an average slip rate of 0.2 mm yr^{-1} for much of the Late Pleistocene (Hoover 1974); however, maximum slip rates could have been much higher during this interval. Fault scarps developed in the 11-ka Tabernacle lava field are 15.2 m high (Hoover 1974), however Hecker (1993, citing Oviatt, private communication, 1988) notes that the Tabernacle flows may drape the fault scarps and not be cut by them. In either case, the maximum fault slip rate on the faults in the Tabernacle field is still 15.2 m in 11 ka, or 1.4 mm yr^{-1}. Hoover (1974) also measured 6.1 m of displacement in basalts of the Ice Springs field. An exact age of the Ice Springs field is unknown, however, stratigraphic arguments place it between 3 and 4 ka (Hoover 1974). The maximum slip rate on the Black Rock fault zone in the late Holocene is ∼2.0 mm yr^{-1}.

A9 Drum Mountains scarps (Sevier Desert)

The Drum Mountains scarps cut Pleistocene and Holocene deposits, most of which are syn- or post-Bonneville (∼17 ka) in age, but at least one unit consists of pre-Bonneville alluvial fans (Oviatt 1989; Hecker 1993). The MRE probably occurred between 7 and 10 ka (Bucknam & Anderson 1979a; Crone 1983). An early Holocene age of the MRE is consistent with faulted Provo level shorelines (13.5 ka; Crone 1983). The NVTD is difficult to determine because the fault zone contains both east- and west-dipping structures. Crone (1983) determined a stratigraphic throw of 3.7 m from a single-event trench exposure, with displacement varying from 0.7 to 7.3 m along the fault zone, indicating that more than one event may have produced the scarp offset (Crone 1983). Based on a throw of 3.7 m during the MRE at 7 to 10 ka, the maximum Holocene vertical slip rate is 0.43 to 0.37 mm yr^{-1} and the maximum rate since 18 ka is 0.2 mm yr^{-1}. If the 7-m offset has been produced since ∼7 to 10 ka, the maximum Holocene slip rate is 0.7 mm yr^{-1}, but this is most likely an overestimate of the slip rate. A longer term vertical displacement rate is based on fault scarps developed in Pleistocene lacustrine deposits (Qlg2; Oviatt 1989) and the Pleistocene Smelter Knoll basalt flows (Qvb2; Oviatt 1989). The age of the Smelter Knoll basalts is not well known, with age estimates ranging from 30 to 300 ka (Hoover 1974; Turley & Nash 1980). Therefore, the long-term vertical displacement rate may lie between 0.23 to 0.023 mm yr^{-1}. Seismic reflection and drill hole data suggest that the Drum Mountains faults have been active long enough to produce an offset of at least 46 m.

A10 House Range fault

The House Range fault scarp is pre-Holocene in age and cuts Bonneville deposits with an NVTD of 1.4 m (Piekarski 1980; Sack 1990; Hecker 1993), resulting in a vertical displacement rate of 0.12 to 0.08 mm yr^{-1}. Ertec Western, Inc. (1981) determined a scarp height of 2.5 m for the same scarp, which results in a slightly higher maximum slip rate of 0.14 to 0.21 mm yr^{-1} since 12 to 18 ka.

The Cenozoic displacement along the House Range fault is ∼2 to 3 km, based on the 10 to 15° tilt of Cambrian strata on the east side of the House Range and apatite fission-track ages of 32 to 70 Ma from near the foot of the range front (Stockli 1999). Modelling of these data by Stockli (1999) indicates that cooling and exhumation may have occurred as recent as early to middle Miocene (20 to 15 Ma). We assume that all of the exhumation was directly related to unroofing along the House Range fault (dip 30°), resulting in a maximum vertical rate of 0.2 mm yr^{-1} since 15 Ma. Most likely the rate was a lot higher over a much shorter time interval between 15 and 20 Ma.

A11 Schell Creek Range (Spring Valley fault)

In Spring Valley, late Pleistocene alluvial fans and late Pleistocene and Holocene shorelines have been faulted (Dohrenwend *et al.* 1992). The highstand shoreline is offset by ∼1 m (Dohrenwend *et al.* 1992). Assuming that the age of this shoreline is similar to the Lake Bonneville highstand (∼17 ka), the Holocene vertical slip rate is 0.1 mm yr^{-1}. Along the main Spring Valley fault, mid- to late Pleistocene alluvial deposits are faulted ∼5 m. Fault-scarp analysis indicates that the MRE probably occurred prior to 18 ka and likely between 20 and 30 ka (Haller & Machette, unpublished data), based on the methods of Bucknam & Anderson (1979a), yielding a maximum slip rate estimate of 0.25 mm yr^{-1}. A longer term average slip rate based on these data is 0.04 to 0.013 mm yr^{-1}, assuming that the 5-m offsets are as old as mid- to late Pleistocene (130 to 200 ka; e.g. at Piermont Creek, Friedrich, unpublished data).

dePolo (1998) empirically determined the vertical fault slip rates for normal faults in the Great Basin, including the Spring Valley and Egan Range faults. dePolo (1998) defined the Spring Valley and Egan Range fronts as lacking active triangular facets and assigned vertical slip rates ranging from 0.003 to 0.07 mm yr^{-1}. A minimum vertical slip rate of 1 mm yr^{-1} for 10^5 to 10^6 yr is needed to produce active fault facets; remnant facets, however, can be maintained with a vertical uplift rate as low as 0.1 mm yr^{-1} (dePolo 1998). The presence of a remnant 30-m scarp along the Schell Creek Range front suggests that slip on the Spring Valley fault may have been ∼0.1 mm yr^{-1} for the past ∼300 ka.

A minimum estimate for the long-term vertical slip rate along the Spring Valley fault is based on seismic reflection lines, drill hole data and estimated age of the basin fill (Gans *et al.* 1985; Miller *et al.* 1999). Gans *et al.* (1985) estimated a horizontal extension of 8 to 9 km across Spring Valley, based on the apparent offset of the Precambrian McCoy Creek Group, and a dip-slip separation of 12 km based on offset Cambrian and Precambrian strata. Assuming

a dip of 30° for the fault, the throw across the fault is ∼6 km and the long-term vertical slip rate is 0.25 mm yr^{-1} since the onset of faulting along the Spring Valley fault (e.g. Lee 1995).

A12 Egan Range fault

Fault scarps along the eastern Egan Range front cut early to middle Pleistocene deposits (130 ka to 1.5 Ma; Dohrenwend *et al.* 1992), but Holocene deposits are not cut (Ertec Western, Inc. 1981). The surface height of the scarps is 10 m with a scarp slope angle of 10° (Ertec Western, Inc. 1981), which suggests that the age of the scarp may be significantly older than 100 ka (Bucknam & Anderson 1979b). A long-term maximum vertical displacement rate of ∼0.1 mm yr^{-1} can be calculated from these data. The Cenozoic vertical displacement across the Egan Range fault is >1 km, based on sedimentary basin thickness (Gans *et al.* 1985). Assuming that extension started as early as Oligocene, based on a 27.4-Ma vitric tuff identified near the base of the syntectonic valley fill (Anderson 1983), the minimum vertical displacement rate is 0.04 mm yr^{-1}. If extension started at roughly the same time as in the Spring Valley (∼15 Ma; Lee 1995), the long-term vertical displacement rate would be 0.067 mm yr^{-1}.